

See discussions, stats, and author profiles for this publication at: <https://www.researchgate.net/publication/317371482>

Review on Modeling and Simulation of Blast Furnace

Article in Steel Research International · January 2018

DOI: 10.1002/srin.201700071

CITATIONS
132

READS
5,278

3 authors:



Shibo Kuang
Monash University (Australia)

122 PUBLICATIONS 3,637 CITATIONS

[SEE PROFILE](#)



Zhao Yang Li
Shandong Iron and Steel Group CO. Ltd. 中国钢铁集团有限公司

20 PUBLICATIONS 386 CITATIONS

[SEE PROFILE](#)



Aibing Yu
UNSW Sydney

885 PUBLICATIONS 39,822 CITATIONS

[SEE PROFILE](#)

Some of the authors of this publication are also working on these related projects:



Cobaltate Thermoelectrics [View project](#)



Numerical Study of Aerosolisation of Carrier based Dry Powder Inhalation Systems [View project](#)

Review on Modeling and Simulation of Blast Furnace

Shibo Kuang,* Zhaoyang Li, and Aibing Yu*

The design and control of blast furnace (BF) ironmaking must be optimized in order to be competitive and sustainable, particularly under the more and more demanding and tough economic and environmental conditions. To achieve this, it is necessary to understand the complex multiphase flow, heat and mass transfer, and global performance of a BF under different conditions. Mathematical modeling, often coupled with physical modeling, plays an important role in this area. This paper reviews the recent developments in this direction. The emphasis is given to mathematical models for different BF regions from the top charging system, body, and finally down to raceway and hearth. The needs for the further research and developments are also discussed.

1. Introduction

Blast furnace (BF) ironmaking is the most important technology by which hot metal is rapidly and efficiently reduced from ferrous materials. In an integrated steelwork, BFs together with the associated units (pelletising-sintering machine and coke oven) represent about 90% of the CO₂ emission^[1,2] and 70% of the energy consumption.^[3] Therefore, it is important to minimize the rate of reducing agent and to make full use of energy in the BF ironmaking process. Essentially, this requires that the heat exchange and chemical reactions between different phases proceed properly in every region of a BF. In pursuit of such a goal, extensive experimental and numerical efforts have been made in the past to study the in-furnace multiphase flow, heat and mass transfer, and global performance of BFs, toward achieving reliable, cost- and energy-effective, and low-emission production ultimately.

A modern ironmaking BF is a high-temperature moving bed reactor involving counter-, co-, and cross-current flows of gas, liquid, solid, and powder, coupled with heat and mass transfer and chemical reactions.^[4,5] Specifically, in the BF practice, the burden materials consisting of coke, ore, and flux particles are charged into the furnace, in most cases layer by layer using either a bell or bell-less top. Meanwhile, the oxygen-rich hot blast/air is introduced from the tuyeres at the lower part, forming void zones known as raceway and there combusts coke to generate

reducing gases and smelting heat. During the burden descent, the ore is reduced and melts in the cohesive zone (CZ) forming liquid slag and iron by the ascending gas. The liquids then percolate through the coke bed in the form of droplets/rivulets in the dripping zone to the hearth, and are periodically drained out through a taphole. Also, the unburnt coal as a kind of powder resulting from the pulverized coal injection (PCI) operation via the tuyeres may leave the raceway region to the upper part through gas entrainment. According to these features, a whole BF can be divided into four main regions^[5]: burden top charging system, hearth, raceway, and main body composed of lumpy (dry) zone, cohesive zone, dripping (wet) zone, and deadman. In these regions, the phases involved are present at different length scales like discrete coal/ore/powder/droplet/rivulet, as well as continuous gas/liquid. Furthermore, they experience intensive interactions with each other in terms of flow, heat and mass transfer under high temperature and high pressure. In such a harsh and complex environment, it is impossible to physically access the details of the multi-scale in-furnace states that govern BF performance, especially for the commercial scale furnaces.

In recent years, in line with the development of computational technology, mathematical modeling, often coupled with physical modeling, has become an attractive alternative.^[6–8] It has been increasingly used to study localized and/or global multiphase flow and thermochemical behaviors inside BFs. Generally speaking, the existing approaches can be discrete- or continuum-based with respect to the solid phase, which are represented by discrete element method (DEM) and two-fluid (or multi-fluid) model (TFM), respectively.^[9] Because of the complexity of BF, it is yet difficult to use one kind of numerical model to describe the entire BF process, leading to the potential trends in the development and application

* S. Kuang, A. Yu, Z. Li
Laboratory for Simulation and Modeling of Particulate Systems,
Department of Chemical Engineering, Monash University, Clayton, VIC
3800, Australia
Email: shibo.kuang@monash.edu

of multi-scale BF models toward tackling practical problems. In this direction, both discrete and continuum models have, therefore, attracted many interests. In 1993, Yagi^[10] summarized the formulations of continuum models for four-fluid flow, extended from the previous models for single-, two-, and three-phase flows. Dong et al.^[11] reviewed the model developments in aspects of formulation, validation, and application for the gas-solid, gas-liquid, gas-powder, and multiphase flows inside BFs mainly in the period between 1993 and 2007, where both continuum and discrete studies were considered. Ueda et al.^[12] in 2010 and Ariyama et al.^[13] in 2014 further discussed the new efforts reported for the discrete simulation of BF, respectively. However, the previous reviews did not pay much attention to the modeling efforts dedicated to hearth^[14–29] and raceway,^[30–45] of which the performance plays a critical role in determining BF campaign life, as well as operation and maintenance costs. Also, considerable model developments based on either discrete or continuum approach have been made recently. These include, for example, the continuum modeling of layered structures of ore and coke and their impacts on CZ behaviors and global BF performance^[46–50] and three-dimensional (3D) multiphase flow and thermochemical characteristics of BF processes,^[51,52] the discrete simulation of cohesive zone,^[53–55] liquid trickling flow in the dripping zone^[56–58] and coupled flow, heat and mass transfer,^[59–62] as well as the development of large-scale simulation capability,^[63,64] and multi-scale modeling strategy.^[65–67]

This paper reviews the mathematical modeling and simulation of BF processes, with special reference to the formulation, validation, and application of the recent developments. It covers all of the BF regions, including burden top charging system, main body, raceway, and hearth, aiming to give a full picture about BF modeling. The paper is structured as follows: In Section 2, the model frameworks are outlined with respect to continuum and discrete treatments of different phases as well as multi-scale modeling strategy. In Section 3, the numerical studies of key transport phenomena are discussed, respectively, for each of the four regions. The emphasis is given to the recent advances in modeling technique and model application. In Section 4, the development of large-scale simulation approaches is discussed in handling full scale BFs. Section 5 provides a summary and discusses some needs for future research and development.

2. Framework for Mathematical Modeling

BF ironmaking often involves phenomena at different time and length scales, which requires different approaches to model, as demonstrated in Figure 1. Here, the micro scale is at a particle level, the process scale represents the whole blast furnace, the macro scale is much larger than particle



Dr. Shibo Kuang obtained his Ph.D. in 2009 from School of Materials and Metallurgy, Northeastern University, China. In 2005, he as an exchanging Ph.D. student joined SIMPAS which was established by Prof. Aibing Yu at UNSW and later relocated to Monash University. Dr. Kuang became a postdoctoral fellow in SIMPAS in 2010 and then a research fellow in 2015 and till now. His research has focused on the development and application of discrete- and continuum-based computer models to particle-fluid systems for gaining better process design and control, with special reference to particle transportation and separation as well as reacting flows.

size, but still very small compared than the furnace, and the meso scale lies between the micro and macro scales. Correspondingly, the existing numerical approaches for BFs can be generally classified into two categories: continuum approach at a macroscopic level and discrete approach at a microscopic level. The former is typically represented by TFM, where the phases are generally considered as fully interpenetrating continuous media and described by separate conservation equations with appropriate constitutive relations and interaction terms representing the coupling between phases. This approach has been used to model the behaviors of gas, solid particles (i.e., coke and ore), and powder (unburned pulverised coal) in the shaft and raceway and the molten slag and iron in the hearth (see, e.g., refs.[19,31,38,42,68–70]). Its general governing equations, solved by the traditional Computational Fluid Dynamics (CFD), are the conservation of mass and momentum in terms of local mean variables over a computational cell, given by

$$\frac{\partial}{\partial t}(\varepsilon_i \rho_i) + \nabla \cdot (\varepsilon_i \rho_i \vec{u}_i) = 0 \quad (1)$$

and

$$\frac{\partial}{\partial t}(\varepsilon_i \rho_i \vec{u}_i) + \nabla \cdot (\varepsilon_i \rho_i \vec{u}_i \vec{u}_i) = -\varepsilon_i \nabla p + \nabla \cdot \vec{t}_i + \varepsilon_i \rho_i \vec{g} + \sum_j \vec{F}_i^j \quad (2)$$

where i denotes different phases such as gas, solid, liquid, and powder; ε_i , ρ_i , and \vec{u}_i are the volume fraction, density, and velocity of phase i , respectively, and \vec{F}_i^j represents the interaction forces between gas and solid, between gas and liquid, between gas and powder, between solid and liquid, between solid and powder, and between powder and liquid.^[11] The correlations for calculating these interaction forces have been formulated mainly based on extensive experimental data, for example, the Ergun equation^[71] and its variants,^[11] which are widely used in the BF modeling

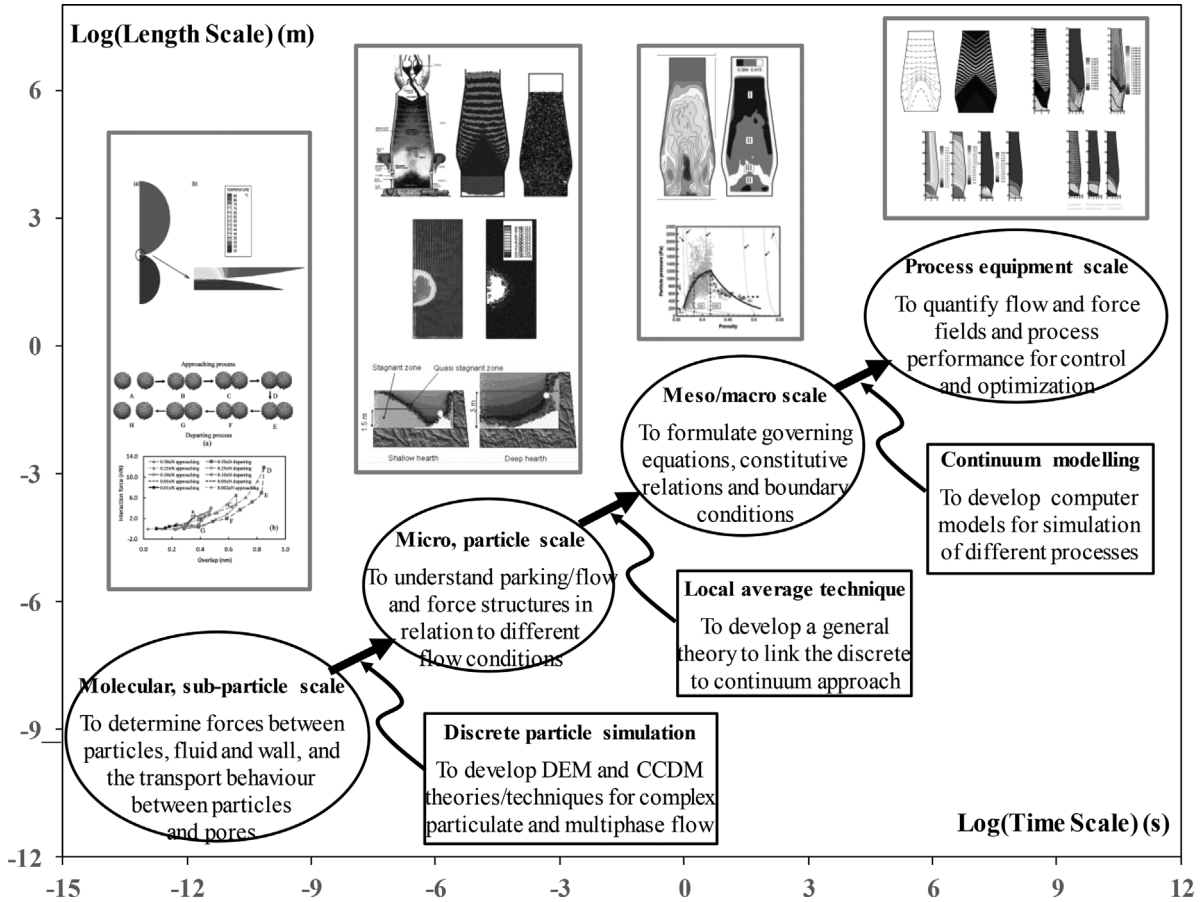


Figure 1. Multi-scale approach^[7] in the modeling of BF ironmaking process.

and expressed as:

$$\vec{u}_i^j = -(\alpha_i \rho_i |\vec{u}_i^j| + \beta_i) \vec{u}_i^j \quad (3)$$

where α_i and β_i are the coefficients in Ergun Equation. Alternatively, sub-particle approaches such as MD (Molecular Dynamics), FEM (Finite Element Method), and LB (Lattice Boltzmann) models have been increasingly used to establish the correlations to describe different interaction forces (see, e.g., refs.[72–74]). Note, that these sub-particle studies often tackle general applications rather than the specific BF process, hereby they are not further discussed in this review.

The discrete approach is typically represented by DEM, where the phases are discrete atoms for gas or liquid and particles for solid phase. DEM can, hence, simulate fluid flow at an atomic or particle scale. It has been widely used to model burden charging process, solid flow in the shaft and hearth, raceway formation, coal combustion, powder percolation, and liquid trickling flow (see, e.g., refs. [30,54,56,67,75–80]). To be computationally efficient in simulating particle-fluid flow, DEM for particles is coupled

with CFD for the fluid (gas and/or liquid) phase (CFD-DEM),^[19] which is also named as CCDM (Combined Continuum and Discrete Model) in the literature. In the DEM approach, the translational and rotational motions of a particle are determined by Newton's second law of motion, that is,

$$m_i \frac{d\vec{v}_i}{dt} = \sum_{j=1}^{k_i} (\vec{f}_{c,ij} + \vec{f}_{d,ij}) + \vec{f}_{s-f,i} + m_i \vec{g} \quad (4)$$

and

$$I_i \frac{d\vec{\omega}_i}{dt} = \sum_{j=1}^{k_i} (\vec{T}_{t,ij} + \vec{T}_{r,ij}) \quad (5)$$

where m_i , I_i , \vec{v}_i and $\vec{\omega}_i$ are the mass, moment of inertia, translational, and angular velocities of particle i , respectively; t is the time; k_i is the number of particles in contact with particle i ; $m_i \vec{g}$ is the particle gravity; \vec{f}_c , \vec{f}_d , and \vec{f}_{s-f} are the elastic contact force, viscous contact damping force, and particle-fluid force, respectively; $\vec{T}_{t,ij}$ is the torque acting on particle i due to particle j arising from the tangential force,

and $\vec{T}_{r,ij}$ is the rolling friction torque. The details of these forces and torques can be found elsewhere.^[7]

Generally speaking, the continuum approach is more suitable for process modeling and applied research because of its computational convenience and efficiency. However, the main limitation of its application is the lack of reliable constitutive correlations. Some global assumptions and arbitrary treatments, therefore, have to be made in this approach.^[68,81] Another shortcoming in the continuum modeling is that the effect of the microstructure is ignored. These problems can be overcome by DEM-based approaches, which have the advantage that there is no need for the complex constitutive relations between the stress and strain tensors for discrete particles under different flow conditions. Moreover, it can generate microscopic information such as the trajectory of and forces acting on individual atoms or particles, which is important to understand the underlying mechanisms.^[7,8] However, DEM-based simulations are computationally too demanding to consider a real BF, where the number of particles can be billions. The averaging theory at a meso scale is promising to overcome the above problems. By use of an averaging procedure, a discrete particle system can be transformed into a corresponding continuum system, leading to the establishment of balance equations of mass, linear momentum, and angular momentum for continuum-based modeling. Such a procedure can be based on volume, time-volume, or weighted time-volume averaging method, as reviewed by Zhu et al.^[7] Under the support of a proper averaging theory, the macroscopic properties of solid flows such as mass density, velocity, angular velocity, stress tensor, and couple stress tensor can be investigated based on the microscopic information generated by DEM simulations.^[66,82] Moreover, based on such studies, constitutive correlations can be developed to improve continuum models. In this direction, some efforts have been made by Zhou et al.^[67] in their study of BF.

Both the continuum and discrete based model frameworks have been used in the studies of BF processes, depending on the investigators' preference and/or research needs. In the following, the studies are briefly reviewed, with major findings discussed. For convenience, this discussion is divided into four parts, corresponding to the four main regions of a BF, that is, hearth, raceway, burden top charging, and body and the strategy for BF process modeling (see Figure 2).

3. Modeling and Simulation of Different BF Regions

3.1. Hearth

The hearth is an important part of the BF process, as reflected from the following facts: (i), the main product,

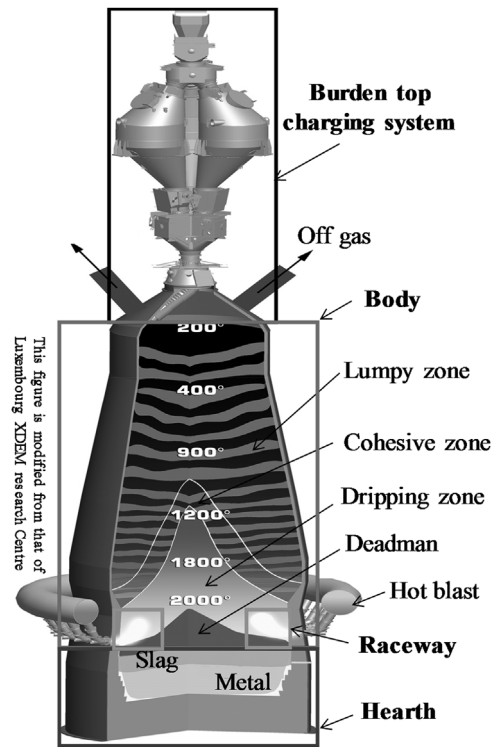


Figure 2. Regions considered and strategy in BF modeling: the burden top charging system and raceway as inlets for the body whose output is the input for the hearth.

hot metal, assumes its final temperature, and composition in this region; (ii), the slag flow and its effective removal affect the stability of the BF operation and productivity; (iii), stagnant zone causes irregular burden descending and abnormal hearth erosion (e.g., the so called elephant foot) if it becomes like solid rock or inactive; and (iv), the wear of hearth refractories is widely recognized as the main limitation for a long campaign life. Therefore, it is critical to control the flow, and heat and mass transfer within the hearth for maximizing the furnace campaign life, as well as securing product quality and furnace stability. Many numerical studies have been carried out in this respect, leading to the development of diverse hearth models.

3.1.1. Flow and Heat Transfer

3.1.1.1. Continuum Modeling: Modeling the hot metal flow, with or without conjugate heat transfer between liquid and solid wall during the tapping process, is one of the main modeling efforts for hearth. This has mainly been done based on continuum models.^[19,21,23,26,27,83–90] Generally, these models consider a single-phase flow, treat the coke bed as porous media, neglect movements of coke and liquid interface, and regard the flow and heat transfer as under a steady state. Also, Finite Volume Method (FVM), which is widely used in CFD computation, was

mainly used to solve the mass, momentum, and energy conservation equations, although some studies used FEM to predict the heat transfer through refractory walls for given profiles.^[91,92] Furthermore, in some CFD models, some specific treatments, as detailed below, have been introduced for coke bed and nature convection.

In practice, the coke bed in the hearth may float in the hot metal (viz. floating coke bed), rest on the refractory pad near the middle of hearth (viz. sitting coke bed with coke free gutter), or fill the hearth completely (viz. sitting coke bed). Under such conditions, the patterns of hot metal flow present significant differences. For example, in a fully sitting bed, the liquid flows through the coke bed toward the taphole during drainage, whereas in a floating bed, the liquid may pass through the coke free zone at the bottom of the hearth. In response to the complex structure of coke bed and its important roles, Guo et al.^[19] further developed the laminar flow model of Panjkovic et al.^[85] by taking into account turbulence using the $k-\epsilon$ turbulence model and modified the turbulence model to consider the effect of microscopic flows around coke particles. They also introduced a thermal dispersion term, which is expressed as a function of the Peclet number and the ratio of thermal conductivity between the solid structure and the fluid for the determination of thermal conductivity. These developments provide a way to consistently treat the coke bed and coke free zone.

In the hearth, natural convection occurs due to the variation of fluid density with temperature. It may be significant because the hot metal flow is generally slow, caused by the large resistance from coke bed and the large dimensions of hearth relative to taphole. Guo et al.^[19] modeled the natural convection, combined with the use of fine CFD grids for numerical stability. However, their model under-predicted the measured temperature.

Conversely, Huang et al.^[88] proposed a model without natural convection. Their model somehow predicted the measurement reasonably, which however must be facilitated by numerical fitting. More recently, Komiyama et al.^[27] based on a systematic model study, revealed that these conflicting results are mainly attributed to the selection of the permeability in simulations, the critical value of which can demarcate two very different flow patterns. With this realization, the predictions by the model of Guo et al.^[19] can be improved by setting permeability or porosity within a suitable range,^[27] as shown in Figure 3. Here, four hearth conditions are considered: intact firebrick and sitting coke bed (case A), intact firebrick and floating coke bed 500 mm above refractory (firebrick) base (case B), eroded firebrick and sitting coke bed (case C), and eroded firebrick and floating coke bed 500 mm above refractory (ceramic cup) surface (case D). In all the cases, the calculated and measured results are in better agreement for a “low permeability” coke bed (porosity = 0.3) compared to a “high permeability” one (porosity = 0.35).

3.1.1.2. Discrete Modeling: Different from the continuum modeling of hot metal flow, modeling the solid flow in the hearth has been performed using discrete approaches. Nouchi et al.,^[93,94] by use of a DEM model, first reproduced the key particle behaviors related to the formation of coke bed and coke free zone against the experimental observations. Such studies were also extended to consider the entire BF at a small scale rather than only the hearth.^[95] In particular, Zhou et al.^[78] developed a CFD-DEM model to quantify the effects of the amount of liquid accumulated in the hearth, coke consumption rate, and gas flow rate on the profile of the coke free zone. These effects are obvious, for example, as those shown in

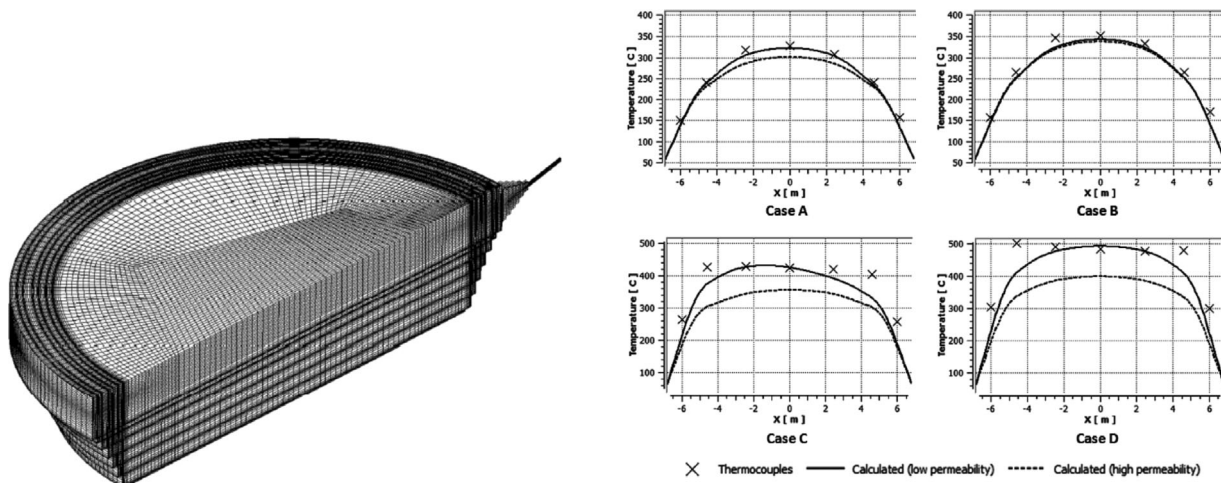


Figure 3. Comparison of the calculated and measured temperatures for Cases A–D: cross dots, measured temperature; dashed lines, calculated temperature for the coke bed with the porosity of 0.35 and the particle size of 30 mm; and solid lines, calculated temperature for the bed coke with the porosity of 0.30 and the particle size of 12 mm.^[27]

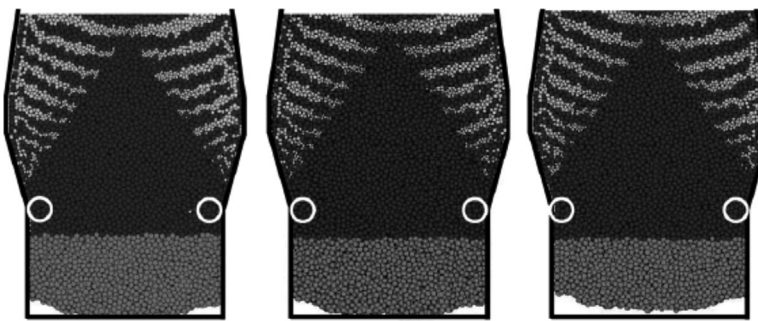


Figure 4. Predicted floating states of the particle bed in the hearth at different gas velocities: a), 0 m s^{-1} ; b), 30 m s^{-1} ; and c), 45 m s^{-1} .^[78]

Figure 4. It reveals that the floating state of the coke bed becomes more obvious in the hearth with increasing gas velocities.

Generally, the DEM-based models can well predict the complex state of the coke bed, which to some degree controls the flow pattern in the hearth but is difficult to model by continuum approaches. However, to date, these discrete models of hearth are based on cold models and do not explicitly consider the liquid flow. Thus, further efforts are needed to develop such models for more realistic applications.

3.1.2. Liquid Drainage

The tapping process is modeled using continuum approaches, having two kinds of formulations. One is the so called VOF (Volume of Fluid) model, where fluids are assumed immiscible and the donor accepted method is used to trace the movement of interfaces.^[15,96–98] Nishioka

et al.^[15,96] combined the VOF model for hearth and the drainage prediction model at a taphole outlet to describe the drainage behaviors and the interface shapes and movement of immiscible fluids having different properties. This integrated model was also extended to consider the heat transfer and the mass transfer of FeO and related chemical reaction and slag solidification during the tapping process.^[97] Figure 5 thus shows the predicted distribution of FeO, which changes slag viscosity and thus drainage stability of slag. Recently, using VOF model, Shao and Saxén^[98] studied the stratified flows of liquid iron and slag along a taphole, where the effect of coke bed was neglected. The VOF-based models are attractive because of its simple formulas and low computational requirements. However, the interfacial force, which is of importance for momentum transfer between the liquids in the hearth, is neglected in the previous VOF models. To overcome this problem, Shao et al.^[25,99–101] developed different Eulerian–Eulerian models for taphole, hearth, or

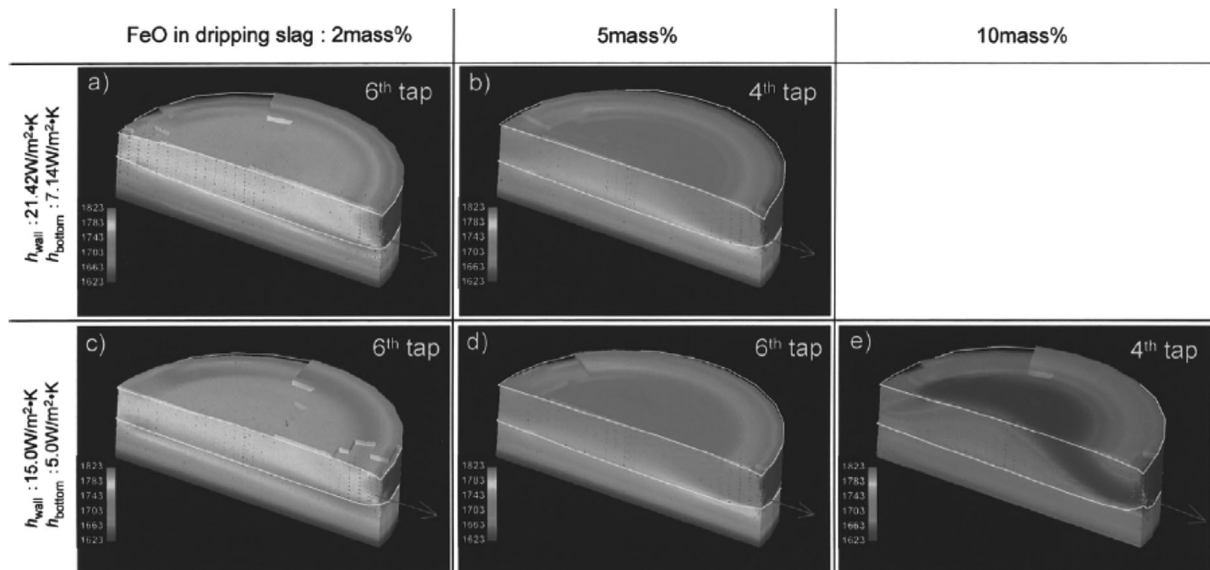


Figure 5. Effect of total heat transfer coefficient of hearth wall and bottom, and FeO concentration in dripping slag on temperature distribution in the hearth at the beginning of the tap.^[97]

both of them to predict the liquid drainage behaviors. In such models, the fluids are assumed penetrable, the geometric reconstruction scheme like Piecewise Linear Interface Calculation (PLIC) is used to locate the interface, and the interfacial forces are considered. Besides the above models, various predictive drainage models have been continuously developed to provide fast predictions under specific conditions.^[29,102]

3.1.3. Lining Erosion

The modeling of lining/refractory erosion of hearth can be categorized into three groups. The first group indirectly estimates the erosion profile according to magnitude of wall stress^[24,103,104] or isotherm^[14,17,91,92] using a continuum model, as discussed in Section 3.1.1.1. Here, the value of isotherm, at which the wall is eroded, is set to 1150 °C for carbon brick and 1350 °C for chamotte brick, determined by the investigation of dissected BFs.^[14] Differently, when the wall stresses are considered for estimating erosion, the locations with high possibility for the occurrence of erosion are qualitatively identified. This is based on the understanding that the wall suffering from large magnitudes of stresses is more vulnerable to erosion.

The second group directly predicts the erosion profile (see Figure 6) by solving the inverse heat transfer through the refractory wall of hearth. In such an approach, FEM is usually used to calculate the temperature, where the wall boundary representing the wear profile is iteratively adjusted until the calculated temperature can match the measurements by the thermocouples embedded in the wall.^[18,105,106] The skull is a layer of iron and/or slag solidified on the inner surface of the hearth lining and provides a barrier between the carbon brick and flowing liquid iron or slag. The FEM approach can also model the formulation of skull, as demonstrated by Zagaria et al.^[105] In their model, the amount of skull is determined by the position of the isothermal curve corresponding to a temperature of 1150 °C in the hearth lining. This temperature corresponds to the solidification of the eutectic Fe–C, and below this temperature, the hot metal is in the solid state. Figure 6 presents the calculated mushroom shaped wear profiles with and without skull. The skull (having

relatively lower thermal conduction) can be identified in the area where the isotherm lines are denser, which means a quick decrease in temperature. Consequently, the formation of skull reduces the erosion of hearth lining, as shown in Figure 6. Zhang et al.^[17] integrated a 1D inverse heat transfer calculation for determining the erosion profile into a 3D CFD model for calculating the hot metal flow and temperature distribution in the hearth and conjugate heat transfer through the wall. This integrated model allows considering the impact of the flow related to coke bed state and other conditions on the erosion profile.

The third group is the CFD models developed to describe the mass transfer in conjunction with the flow and heat transfer to predict the transport phenomena associated with the erosion process. In this direction, Chang et al.^[89] modeled the carbon dissolving behaviors in the coke bed and the transfer of carbon in the hearth based on the calculated hot metal flow and heat transfer, and then estimated the erosion rate which is expressed as a function of liquid velocity, carbon concentration, and liquid temperature. On the other hand, Guo et al.^[22] developed a CFD model to simulate the titanium behaviors in BFs. In their model, the species transport equation of titanium, together with the mass, momentum, and enthalpy equations of molten iron are solved. It takes into account the mass transfer related to chemical reactions for Ti(C,N) formation and uses population balance model to predict the sizes of titanium particles. Therefore, this model can predict the spatial distributions of volume fraction of Ti(C,N) particles, their sizes, and their melting-forming boundary, as shown in Figure 7. This study was further conducted by Komiyama et al.,^[28] who found that the isotherm of the equilibrium temperature of the hot metal can be used as an indicator for the extent and phase of Ti compounds, and on this basis, adjusted this isotherm to control the particle formation in the hearth by either altering the inlet titanium mass fraction or the hot metal pool temperature through systematic simulations. Recently, Zhao et al.^[107] integrated the solidification model based on the melt/freeze enthalpy-porosity technique into the flow

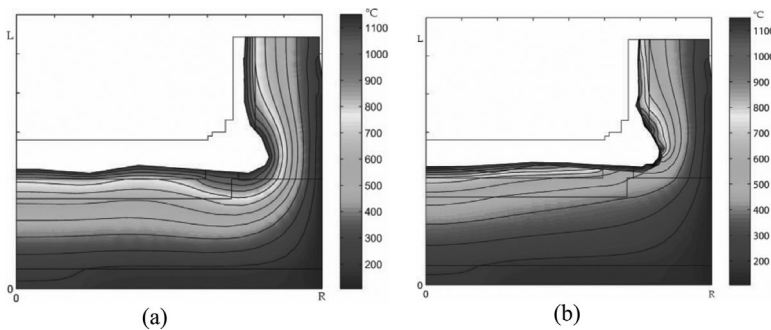


Figure 6. Wear profiles predicted: a) without and b) with skull.^[105]

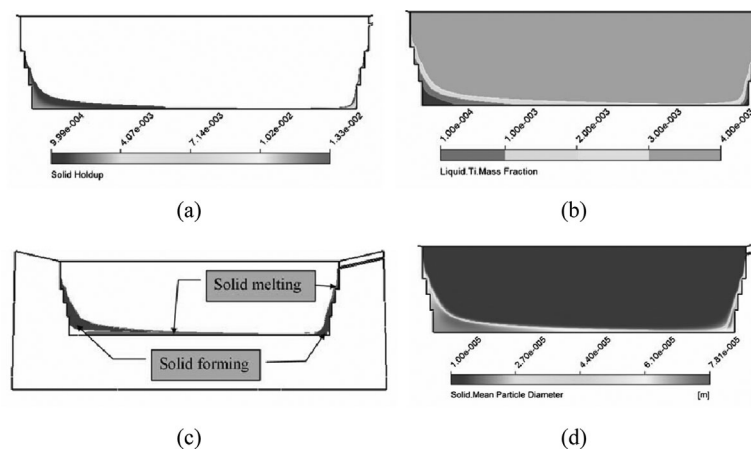


Figure 7. Spatial distributions of a) solid hold up, b) titanium mass fraction, c) regions of solidification and melting, and d) solid particle size.^[22]

and heat transfer models to describe the formation of skull.

Although various modeling efforts have been taken to predict the erosion behaviors of hearth wall, to date, how to directly predict the erosion profile without the support of thermocouple data is not clear. This requires a better understanding of erosion mechanisms in the hearth. Discrete-based hearth models, which currently consider only the solid flow, should be useful in this respect.

3.2. Raceway

In modern BFs, most of the coke and injected supplementary fuels such as pulverized coal (PC) are burnt in raceways to provide heat and reducing gases for this process. The size and shape of a raceway are therefore important in distributing these gases and enthalpy to the lower zones of a BF. Furthermore, these distributions are time-dependent and can be affected by factors such as instability of the raceway boundary and generation of unburnt fines among others. Additionally, the unburnt fines accumulate in the raceway and/or flow into other regions. This situation somewhat deteriorates furnace performance. As such, modeling raceway needs to consider the phenomena related to both raceway formation and fuel combustion. It provides raceway shape and size, burnout of injected fuel(s), spatial distributions of reducing gas velocities, components, and temperatures. This information can be used not only for process control and optimization, but also for investigation of BF body as another important boundary input.

3.2.1. Raceway Formation

3.2.1.1. Discrete Modeling: Xu et al.^[75] first developed a CFD-DEM model to study raceway gas–solid flow and illustrated that this approach can give useful particle-scale

information, such as particle trajectories and forces for a better understanding of raceway phenomena. Feng et al.^[108] extended this work and quantified the effects of solid extraction (corresponding to coke combustion), gas velocity, and solid pressure. They observed a periodic arching and collapsing flow associating with the peeling (expansion) and pasting (contraction) phenomena within a raceway, as well as the increase of raceway size as a result of coke combustion. Nogami et al.^[109] modeled the heat transfer and chemical reactions related to the combustion of coke and PC in their CFD-DEM study of raceway and found that blast temperature and compositions change raceway shape and size. Yuu et al.^[110] developed a combined DEM for coke, CFD for gas, and DMSCM (Direct Simulation of Monte-Carlo Method) for powder to study the phenomena in the raceway of a commercial BF. Using this model, Umekage et al.^[34,111] studied the effects of wall cohesive matter, tuyere angle, wall scaffolding on raceway shape and size. Hilton et al.^[112] demonstrated that particle shape is crucial to the structure and the dynamics of circulation regions in their CFD-DEM simulation of lateral injection of high-speed gas into a packed bed of different shaped particles. Recently, Hou et al.^[113] used a CFD-DEM model to study the raceway behaviors as a result of two lateral jets into a packed bed and found that with increasing superficial gas velocity, a raceway can form only when the bed width is large enough. Generally, the above studies considered the lower part of BF or a box-shaped packed bed at a small scale. Differently, Miao et al.^[45] conducted a CFD-DEM study of a full-scale BF with the regions from the burden surface to the bottom. In their simulations, two different particle configurations were considered at the gas injection velocity from 10 to 25 m s⁻¹, referred to as Model I and II, respectively. The furnace is loaded only with coke particles (density = 920 kg m⁻³) in Model I, but alternative layers of ore (density = 3300 kg m⁻³) and coke (density = 920 kg m⁻³) particles in Model II. Anti-clockwise, clockwise, and plume-like raceways are predicted, as shown in Figure 8.

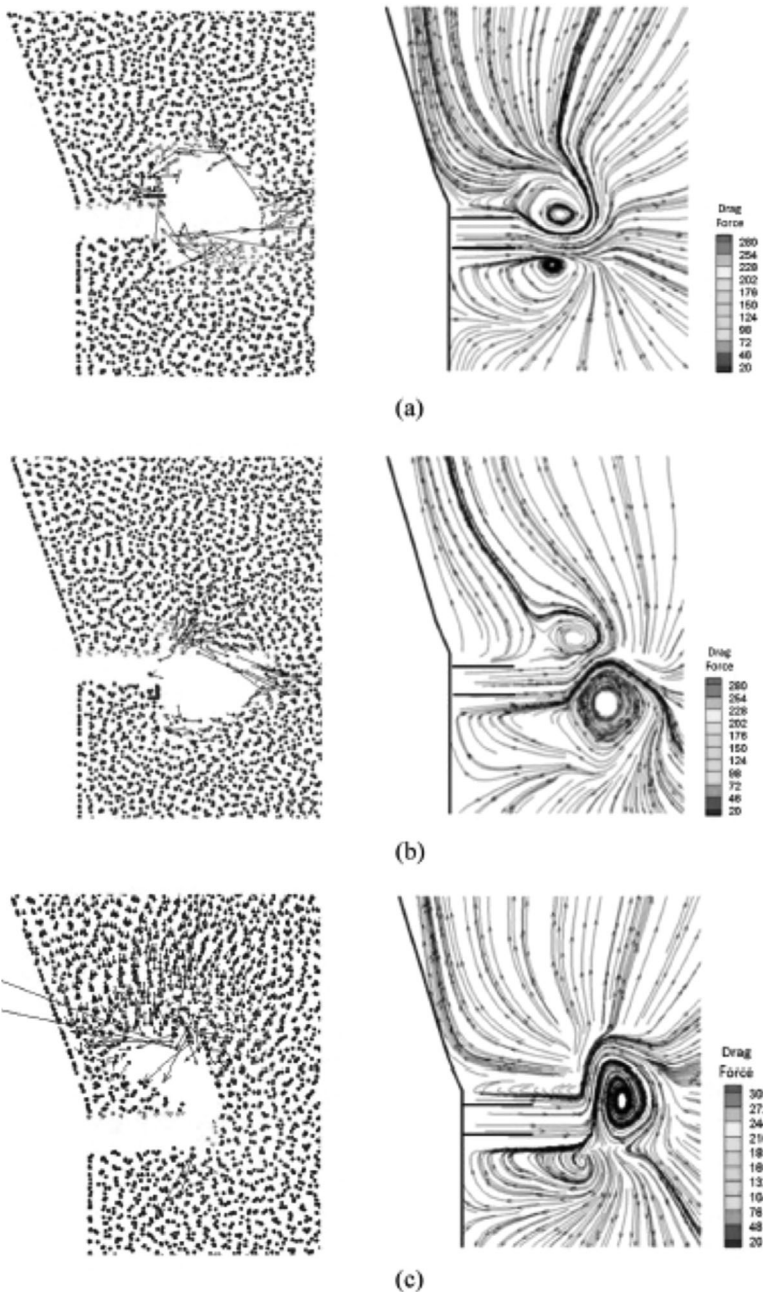


Figure 8. Drag force and particle velocity distributions acting on particles and its corresponding gas streamline (tuyere length = 0.7 m) for: a), anti-clockwise raceway when blast velocity = 14 m s^{-1} in Model I; b), clockwise raceway when blast velocity = 12 m s^{-1} in Model I; and c), plumelike raceway when blast velocity = 21 m s^{-1} in Model II.^[45]

The clockwise raceway is observed at a low gas velocity, where particles are pushed into the packed bed in the clockwise circulation direction, and a clear cavity is formed in front of tuyere. The formation of anti-clockwise raceway occurs when gas velocity is in the medium range and is the result of the dynamic balance between incoming kinetic energy and the bed gravitational energy. The plumelike raceways are generated at a high gas velocity. In this case, the gas flow is large enough to break the restriction of the packed

bed, however, and the raceway top cannot be fluidized easily due to the increased bed weight. A slight peeling and pasting behavior is then formed.

3.2.1.2. Continuum Modeling: In comparison with many CFD-DEM studies as discussed above, the studies based on continuum methods are much fewer. Sarkar et al.^[33] developed a two-fluid model, closed by Mohr Coulomb's law for the solid phase, to predict raceway shape and size.

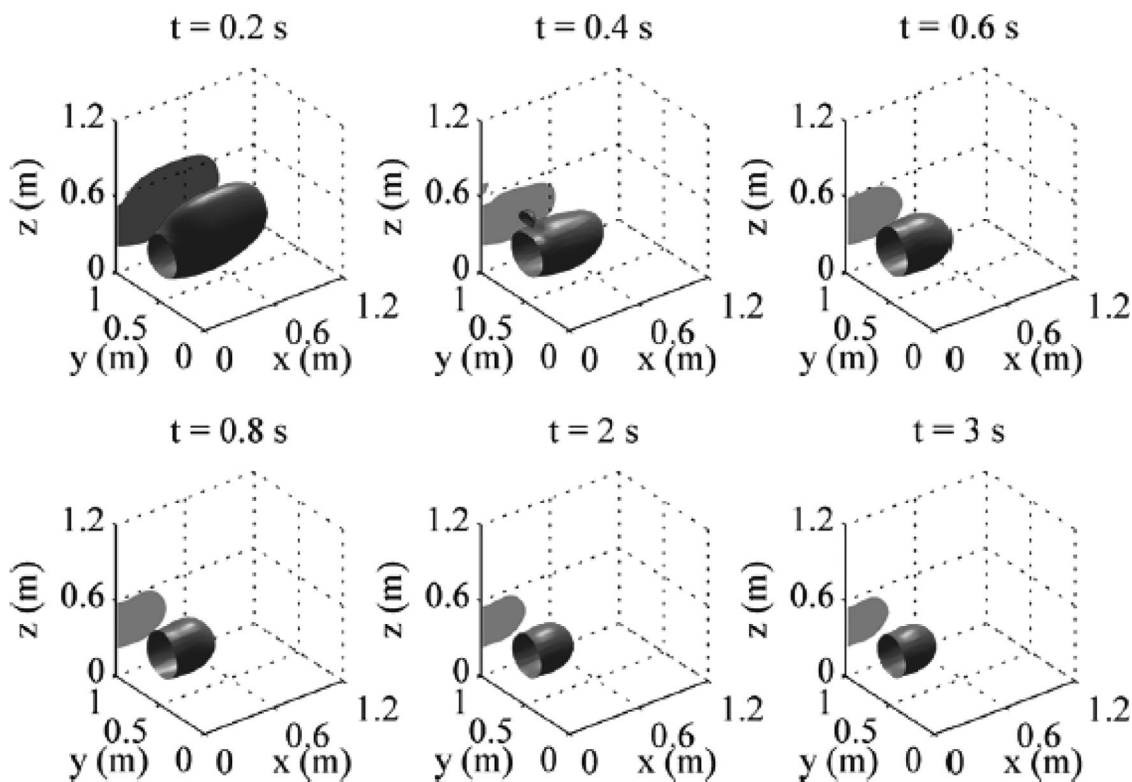


Figure 9. Time evolution of raceway size and shape for a base case in continuum modeling.^[42]

In their study, the raceway boundary is not directly predicted, but identified according to an iso-stress value of the solid phase. The model, hereby, requires the experimental relationship between stress value and gas velocities. Mondal et al.^[31] developed a TFM model facilitated with granular kinetic theory (GKT) to directly predict the boundary of a raceway at different blast velocities, initial bed porosity, and bed heights. Recently, Rangarajan et al.^[42] introduced the friction stress, which is of great importance to dense granular flow, in their TFM-GKT model. By use of the model, they predicted the time-evolution of raceway (see Figure 9) and examined the effects of a series of operation parameters. However, because of the lack of model validation in the previous TFM-GKT studies, it is not yet clear whether or not such models are capable of quantitatively determining raceway shape and size, although their prediction trends against different variables make sense.

3.2.2. Raceway Combustion

The majority of raceway combustion models are based on the combined approach of CFD for gas and LPT (Lagrangian Particle Tracking) for particles (CFD-LPT).^[30,35,37,39,41,114–116] In such a model, individual particles, each of which may represent a single particle or an assembly of particles, are modeled, with the particle-fluid interaction considered but the particle-particle collision ignored. It can be regarded as a simplified CFD-DEM model. However, this simplification can

significantly alleviate the computational effort, and thus CFD-LPT combustion models have already become 3D in 2000s from 1D in 1980s and 2D in 1990s.^[35]

The main modeling efforts here lie in the description of the combustion and associated phenomena in tuyere and raceway. A representative model in this respect is the one developed by Shen and his colleagues.^[30,35,37,39] In their model, the computational domain covers lance, blowpipe, tuyere, raceway, and coke bed, as shown in Figure 10. The blowpipe-tuyere-raceway region is treated as a cavity, the coke bed is treated as porous media, and the size and shape of raceway are determined according to the CFD-DEM results. This model includes the reactions related to: (i), coal combustion (devolatilization, volatile combustion, and char reactions); (ii), gas combustion; and (iii), coke combustion and gasification.^[39] On the other hand, other researchers developed a two-fluid model to predict the combustion process in BFs,^[38,40,44] considering the reactions and computational domain similar to those by Shen et al.^[39]

The combustion models of raceway have been used to generate various useful results. In particular, through numerical and physical experiments, Murai et al.^[114] reported that simultaneous injection of PC/plastics or PC/gas fuels is favorable to improve combustion efficiency remarkably, and 86% of exhaust carbon can be reduced in an optimized BF with top gas recycling and sequestration and fixing of carbon dioxide. Du et al.^[115] based on numerical results, replaced single lance with double-lance

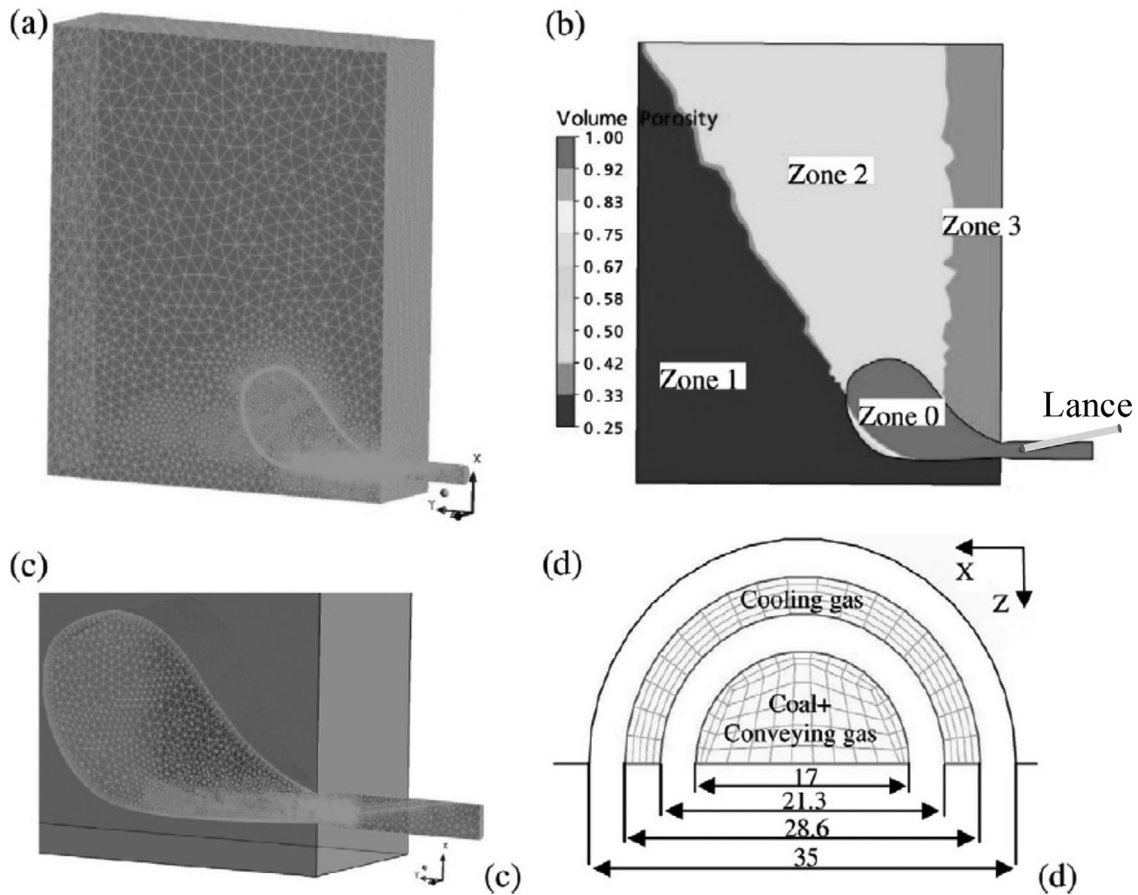


Figure 10. Geometry of the model: a), the whole model; b), porosity distribution; c), blowpipe and raceway; and d), lance tip.^[39]

for the PCI operation in a practical BF. This modification increased the PC injection rate from 110 to 153 kg tHM⁻¹. Shen and his colleagues conducted a series of numerical studies to quantify the influences of the key parameters on coal burnout for PCI operations, including binary and trinary coal blends,^[36,117] coal properties,^[118] and operational conditions such as blast conditions and type of cooling gas.^[37,119] These studies proved that this computer model can indeed be a cost-effective tool to understand raceway combustion phenomena and optimize PCI operations. Recently, some new developments of PCI technologies were numerically assessed, including injection of pulverized biochar,^[41,116] natural gas with PC,^[44] and upgraded brown coals,^[120] confirming the feasibility of such technologies from the viewpoints of numerical experiments.

3.3. Top Burden Charging System

Within a BF, the burden distribution plays an important role because it influences the formation, shape, and location of the cohesive zone, which is critical to the gas flow distribution and the furnace performance. The

prediction of particle behaviors inside this top region helps properly operate the charging equipment to achieve the accurate control of burden distribution. It also provides the basic boundary information to study the burden descent and associated phenomena in the BF body. For a long time, such prediction has mainly relied on the models derived from the motion of a single particle or particle assembly.^[121–124] In recent years, the DEM approach, which considers all individual particles and their interaction with each other, has become a promising tool to guide burden charging operation.^[79,125]

Figure 11 shows a representative application of DEM in simulating the bell-less charging system mainly used in modern BFs. Such a simulation can give the trajectories of and forces acting on particles of various types inside the whole top system and their distribution at the burden surface in the throat including radial distributions of particle sizes and ore-to-coke volume ratios under different conditions. This information can directly be used to guide and optimize charging operations. It can also be used to better understand the complicated particle behaviors to achieve confident BF operations. In particular, during the charging process, segregation occurs inside the charging equipment, during the falling in the off-gas,

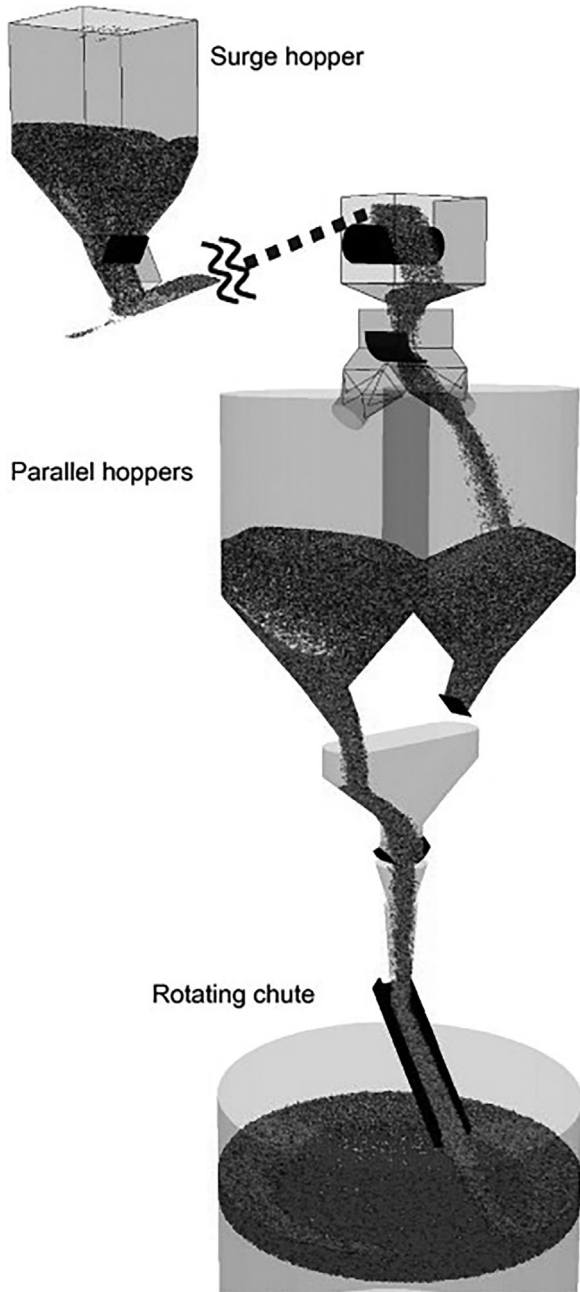


Figure 11. Snapshot of a full model for bell-less type charging process of blast furnace.^[79]

and along the burden surface because of the particles of different sizes, shapes, densities, surface properties, as well as the asymmetrical features of equipment geometry and charging operation. Also, coke collapses when much heavier ore is charged onto coke layers. Both phenomena significantly affect the burden radial distribution and can readily be predicted using DEM charging models over a wide range of conditions.^[79,124–132] Such capability is, however, difficult to achieve by single particle based models.^[121–124] For example, the formulation of coke

layers, although complicated, can be well predicted by the DEM simulations simply based on spherical particles if the friction coefficients are carefully chosen, as demonstrated in the work of Liu et al.^[125] (see Fig. 12). Those investigators also examined the influence of sliding and rolling friction coefficients in the DEM modeling of burden charging process against the measurements. For this purpose, the case where four rings of coke particles are charged and form a steady coke layer is modeled using spherical particles. The results reveal that the predicted burden profile is very sensitive to the two friction coefficients. Under the conditions considered, the rolling friction coefficient should be larger than 0.05, while the sliding friction coefficient larger than 0.5, in order that the calculated and measured results are in good agreement.

3.4. BF Body

BF body is the main area, where the ore is reduced to iron and melts into liquid. This region consists of four flow zones^[5]: (i), lumpy or stack zone where the individual particles of ore do not yet get fused, and the coke and ore layers make a roughly ordered, stratified descent; (ii), CZ where the ore is softened, fused, and eventually melted; (iii) dripping or coke zone which is situated beneath CZ and above the conical deposit of coke known as deadman, serving as the coke supply source for the combustion zone; and (iv), the deadman where the descending behavior of coke is not a continuation from above, and the coke although being continuously updated, has been generally held up for a long time. Descriptions of the burden decent in the shaft, the percolation of droplets/rivulets through the coke bed in the dripping zone and deadman, the behaviors of cohesive zone, as well as the associated flow, heat and mass transfer represent a major modeling effort, as discussed in this section.

3.4.1. Burden Descent

3.4.1.1. Continuum Modeling: The early numerical models for the description of burden descent in BFs include^[68]: (i), viscous flow model where solid flow is treated as a continuous flow of viscous fluid, and the viscosity is often assumed constant; (ii), potential flow model where the descending velocity of solids is assumed to be proportional to the gradient of velocity potential; (iii), kinematic model where the velocity of a particle in the radial direction is proportional to the particle velocity gradient in the axial direction. The comparison of the three models against the measurements suggests that the viscous fluid model is the best in the simulation of solid flow in the cold model of a BF.^[68] However, in these models, the deadman shape has to be prescribed before calculation. Additionally, the effective method to determine solid viscosity has not been fully established for the viscous model. To overcome these problems, a solid

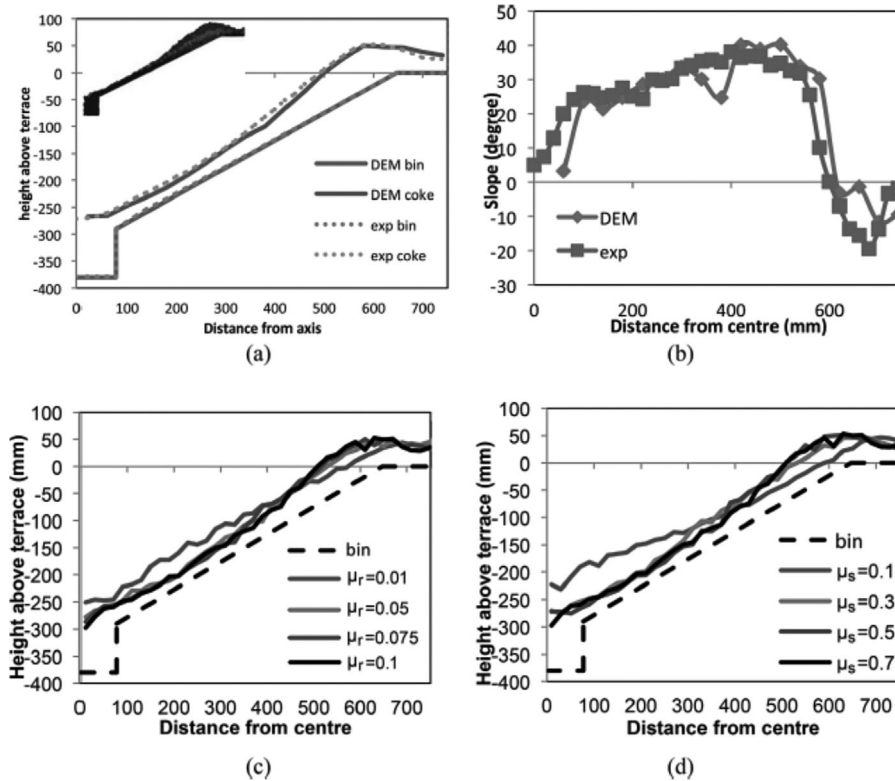


Figure 12. a), Comparison of coke bed results generated from DEM simulation and experiments when chute angle is 42° from the vertical direction; b), coke burden surface slope; c), effect of rolling friction coefficient; and d), sliding friction coefficient on coke layer surface profiles obtained from DEM simulation when chute angle is 42° from the vertical direction.^[125]

flow model based on the hypo-plasticity theory for granular materials, solved by FEM, has been developed by Zaïmi et al.,^[133] and then linked to a multi-fluid BF process model.^[65] Nogami and Yagi^[134] applied the Bingham model, which is the simplest shear rate–shear stress model of plastic fluid, to the viscous fluid model of bulk solid flow in a moving bed. Zhang et al.^[81,135] based on fluid and solid mechanics, developed a mathematical model to describe the solid flow in a BF. In their model, the concept of viscosity is extended to the solid flow to represent the hydrodynamic particle–particle interaction, and the concept of a solid plastic modulus and Coulomb friction relation are employed to describe the frictional contact interaction. Also, a method is proposed to determine the transition between moving and non-moving zones, that is, the profile of stagnant zone. Zhou et al.^[136] later simplified their model by neglecting rate-independent part. This simplified model does not accurately predict the quasi-stagnant zone, which is associated with the strong inter-particle friction and should be described by a more complicated model, as shown by Zhang et al.^[81] On the other hand, it is superior to the early potential, kinematic, or viscous model and is simple to be included in a process model. Recently, Nick et al.^[137] extended the model of Zhang et al.^[81] from 2D to 3D.

3.4.1.2. Discrete Modeling: DEM-based models have been extensively used to describe solid flow in BFs in recent years. Such studies have been reviewed previously^[11–13] and thus are outlined here, with new developments highlighted. Generally speaking, the advantages of the discrete models over the continuum models for solid flow include the following aspects. First, discrete models can realistically predict the solid flow pattern without the global assumptions and arbitrary treatments made for continuum models. For example, the deadman profile, which is challenging to predict for continuum models, is just a simulation outcome.^[76] Secondly, discrete models allow to investigate the transient behaviors of solid flow and associated phenomena resulting from the complex configurations related to, for example, pre-set CZ shape, tuyere closure, sitting/floating state of coke bed, and pre-set wall crab/scaffold.^[67,78] Understanding these transient behaviors is one of main research focused in the previous DEM studies of BFs.^[11–13] Thirdly, discrete models can provide the details of the flow and forces (see Figure 13), as well as the stress states inside BFs with the support of the averaging theory (see Figure 14). Finally, combining the average theory and discrete model helps develop better constitutive relations for continuum model. In this respect, some attempts have been reported by Zhou et al.^[67]

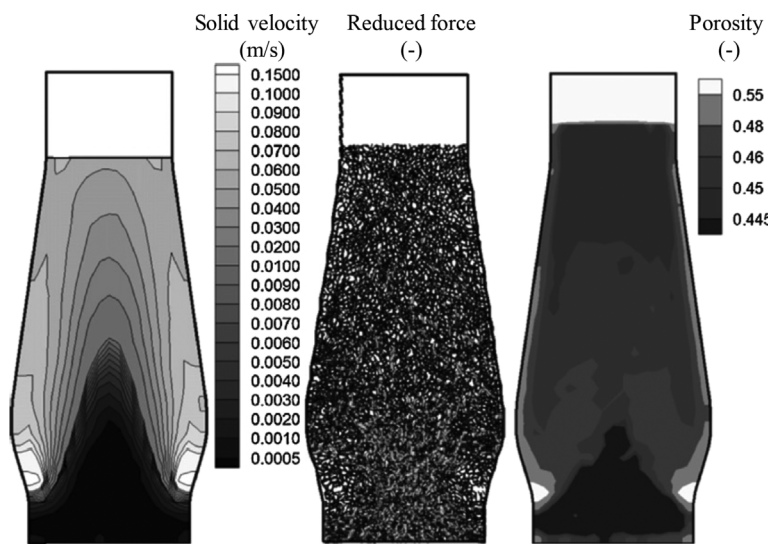


Figure 13. Flow and force parameters obtained from the DEM simulation: a) time-averaged solid flow field, b) contact force network, and c) spatial distribution of porosity.^[76]

Those authors found that typical equations proposed to describe the relationship between solid pressure and porosity become invalid under BF conditions, and accordingly formulated two new equations. Nonetheless, significant efforts are still needed to develop some general constitutive relations to describe the solid flow in BFs.

3.4.2. Trickling Flow of Liquid

Liquid slag and iron generated in CZ trickle down or drop in “icicle” through the coke bed to the hearth, and during

this process, exhibit complicated behaviors, including for example: (i), an unsaturated liquid percolates through a packed bed in the form of rivulets or drops; (ii) localized upward liquid flow, saturation and flooding may occur in CZ; (iii), the effect of packing property on liquid flow is significant; and (iv), slag may exist in a BF as a non-wetting or wetting liquid depending on its reaction with coke, and slag and iron flows may be closely coupled. To describe these features, a few models have been proposed, including the potential flow, probability model,

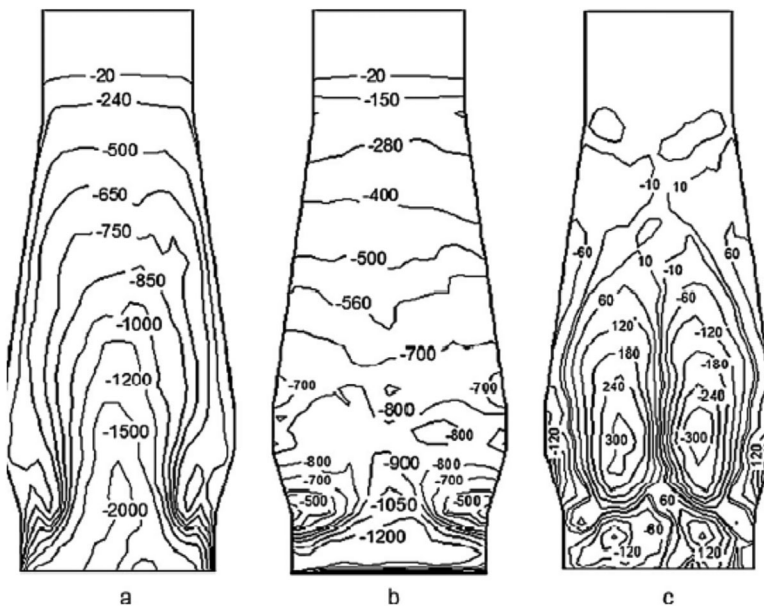


Figure 14. Spatial distributions of a) vertical normal stress, τ_{zz} b) horizontal normal stress, τ_{xx} , and c) shear stress, τ_{xz} (in Pa) in a model BF when solid flow rate is 0.6 kg s^{-1} and gas flow rate is 0.0281 kg s^{-1} .^[66]

probability-continuous model, tube network dynamic model, and force balance model, as reviewed by Yagi^[10] and Dong et al.^[11] Among them, the so called force balance model^[46,138–146] is probably the most promising in describing various liquid behaviors within CZ and coke zones. In such a model, the liquid as rivulets or droplets flows under the influence of gravity, gas drag, and bed resistance, which are in balance with each other. Also, the stochastic motion of droplets, which relates to the packing geometry, is considered by a dispersion sub-model. Based on the force balance, together with the mass balance of the liquid flow, the static and dynamic liquid holdups, liquid velocities, and droplet sizes are iteratively determined. Notably, the predicted droplets usually have different sizes or present a discrete characteristic within the computational domain, depending on operational conditions, packing structures, as well as liquid, and coke properties. This force balance model has been successfully implemented in different BF process models.^[46,145] Below is the representative the force balance model developed Wang et al.,^[139] which includes a liquid flow sub-model featured by the force balance that applies to the discrete liquid flow and a liquid dispersion sub-model to consider the stochastic motion that relates to a complicated packing structure. In the liquid flow sub-model, the equation of motion for the liquid phase can be described by:

$$\mathbf{F}_l^g + \mathbf{F}_l^s + \mathbf{F}_l^{gravity} = 0 \quad (6)$$

where \mathbf{F}_l^g , \mathbf{F}_l^s , and $\mathbf{F}_l^{gravity}$ are, respectively, the gas drag force, bed resistance force, and gravity of a discrete liquid “particle”. In the liquid dispersion sub-model, the stochastic flow phenomenon is described under the following two conditions. First, a stochastic velocity is assumed to be normal to the main flow direction of liquid determined by Equation 6. Secondly, the stochastic velocity has a distribution given by:

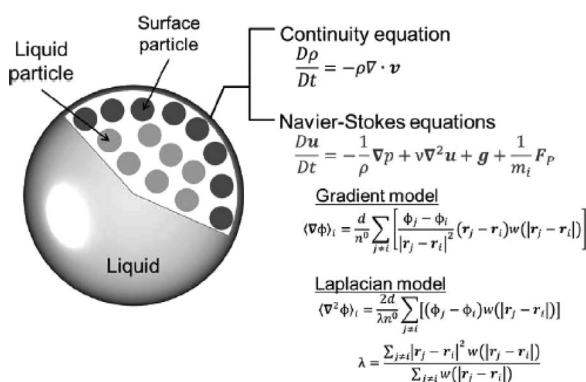


Figure 15. Concept of MPS method and its governing equations.^[13]

$$f(u_s) = \begin{cases} \frac{U_{s0} + U_s}{U_{s0}^2} & (-U_{s0} \leq U_s \leq 0) \\ \frac{U_{s0} - U_s}{U_{s0}^2} & (0 \leq U_s \leq U_{s0}) \\ 0 & (|U_s| > U_{s0}) \end{cases} \quad (7)$$

where U_s is the solid velocity and U_{s0} is the maximum stochastic velocity depending on liquid, gas, and solid properties.

Recently, the Moving Particle Semi-implicit (MPS) method, which is originally for incompressible free-surface flows, has been developed to describe the movement of a liquid and its free surface as a discrete phase.^[147] In such a model, the liquid phase/droplet is considered to comprise MPS particles. The motion of each particle/droplet is described using the continuity equation and Navier-Stokes momentum equations in the Lagrangian coordinates (see Figure 15). The particle-particle collision, representing the surface tension between particles, is calculated using the same algorithm as in the molecular dynamics (MD) method. Nishioka et al.^[148] performed a macroscopic liquid dripping simulation in the region under the blast furnace cohesive zone by the MPS method. Kon et al.^[149] proposed a liquid flow model using the MPS method, in which wetting and interaction with the solid phase are considered by setting packed particles comprising quasi-particles. Natsui et al.^[58] introduced suitable compressibility to MPS to enable the calculation of continuous changes in pressure, and on this basis, coupled the model with DEM which considers different shaped particles. Such models have been used to better understand the liquid flow in the dripping zone, for example, the variation of liquid static holdup in correspondence with different dispersing or coalescing behaviors.^[56] Interestingly, the recent study of Natsui et al.^[58] demonstrated that the particle shape changes the liquid passage velocity and holdup amount, as shown in Figure 16. The MPS simulations, although attractive, were currently performed only at a small scale as they are computationally demanding. Moreover, the model proposed has not considered gas flow and associated heat and mass transfer.

3.4.3. Coupled Multiphase Flow, Heat and Mass Transfer

3.4.3.1. Continuum Modeling: The modeling of BF process heavily relies on the description of the coupled flow, heat and mass transfer in the body from slag surface up to burden surface. Development of a continuum model at a full BF scale has been a continuous effort since 1970s.^[13] Earlier studies had been reviewed by different investigators.^[5,10,11] Generally, in the framework of continuum modeling, the top charging system and raceway are simplified as inlet boundary conditions and

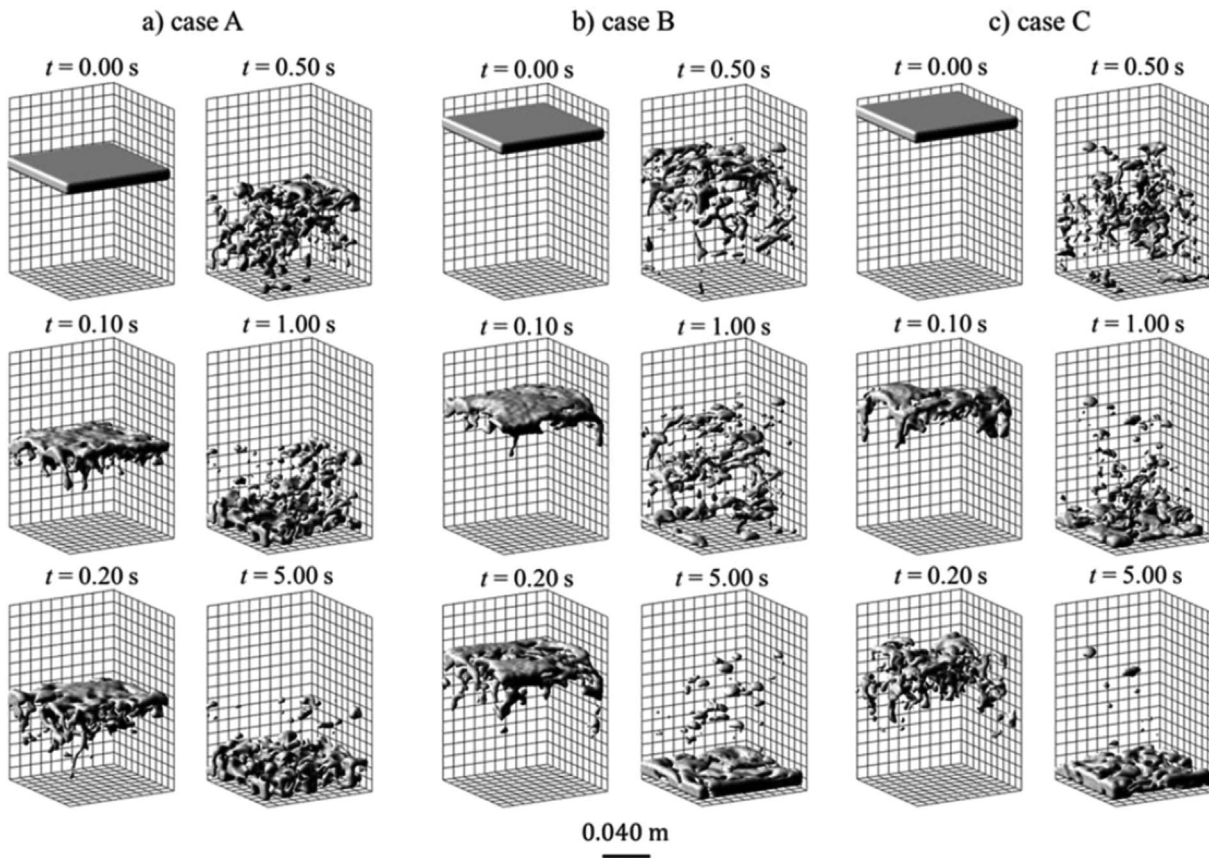


Figure 16. Calculated shape change in liquid interface progressing through a granular medium constituted of: a) cubic-shaped (case A), b) plate-shaped (case B), and c) rod-shaped (case C) elements over time.^[58]

hearth as outlet boundary conditions, so that they can be modeled separately. In the existing continuum models, the gas and solid (consisting of ore, coke, and flux particles) phases are basically considered, while the liquid and powder phases may be explicitly included. A phase consists of one or more components and each component has its own composition and physical properties and is described by a set of conservation equations of mass, momentum, and enthalpy, with the key chemical reactions and the interactions between different phases/compositions considered.^[46,48,51,69,144,150–154] Specifically, for example, the solid phase is modeled by viscous flow model,^[69] its modified version,^[46] kinematic model,^[153] or modified potential flow model^[48]; the liquid phase by continuous model^[69] or force balance model^[46,144]; and either the gas or powder phase is modeled by general fluid dynamic models.^[46,48,51,69,153] Continuum multi-fluid process models have been widely used in the past to assess various ironmaking technologies related to operations (e.g., top gas recycling, and oxygen enrichment), new ferrous materials charging (e.g., scrap, pre-reduced iron ore, carbon composite agglomerates, and hydrogen bearing materials), and injection of auxiliary fuels (e.g., PC, pulverized charcoal, and natural gas), as reviewed by

Yagi^[10] and Dong et al.^[11] Below, the recent new developments and applications are briefly discussed.

CZ is of critical importance for efficient operation of a BF, because its shape and position significantly determine the permeability, fluid flow, gas utilization, thermal and chemical efficiency, and hot-metal quality in the furnace. Therefore, its modeling is key to a BF process model. Different CZ treatments have been proposed, such as isotropic and anisotropic non-layered treatments and layered treatment. Dong et al.^[46] developed a process model where layered CZ is explicitly considered, and on this basis, assessed different CZ treatments. In their model, the layered structure is determined based on the burden distribution at the furnace top (e.g., the ore and coke batch weights as well as the radial distribution of ore-to-coke volume ratios) and the timelines of solid flow. Then, corresponding to the dissection observations, three states are specified for the ore layer within CZ according to normalized shrinkage ratio (Sh_r^*). They are: (i), state I, $0.7 < Sh_r^* < 1.0$ corresponds to the portion with molten state and liquid source in which the ore layer voidage is occupied fully by the liquid phase; (ii), state II, $0.5 < Sh_r^* < 0.7$ corresponds to the combined portion with softening and melting of ores, in which the pressure drop may have

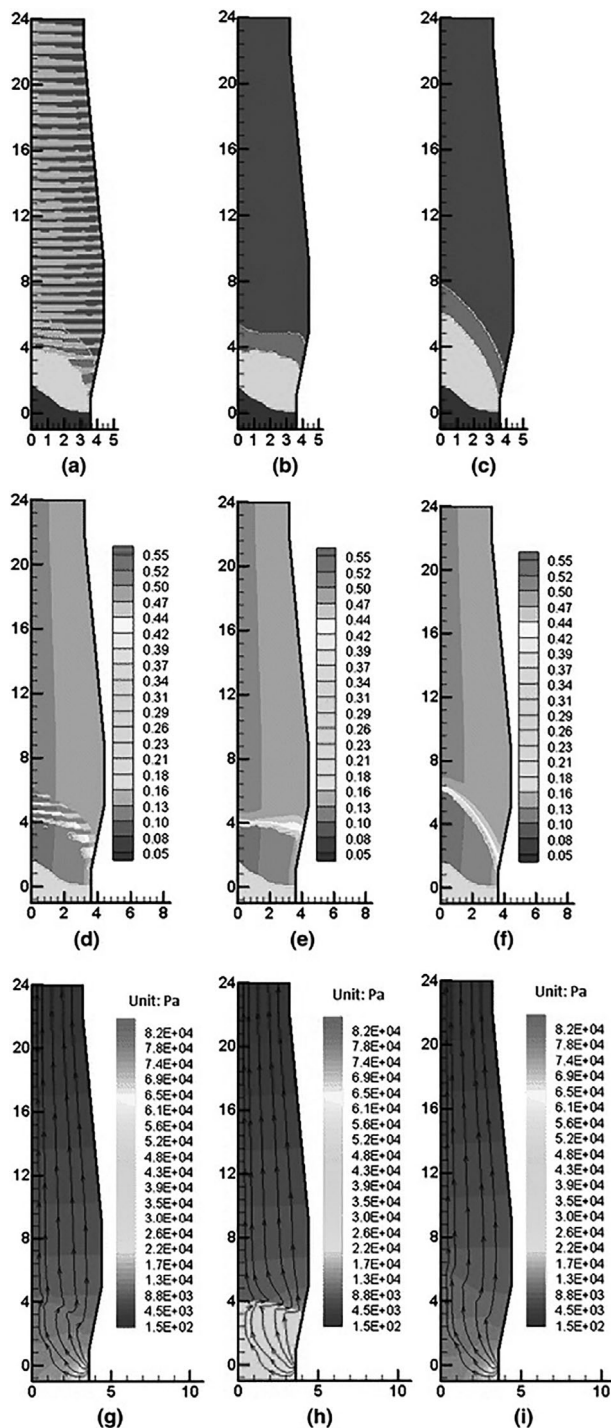


Figure 17. CZ shapes a–c), porosity distributions d–f), as well as pressure drop distribution and gas flow stream line g–i) for the following CZ treatments: left column, layered; middle column, anisotropic nonlayered; and right column, isotropic nonlayered.^[46]

increased significantly; and (iii), state III, $0 < Sh_r^* < 0.5$ corresponds to the softening stage in which macropores of the bed remain open, so the variation of the pressure drop is limited. Accordingly, the porosity and size of ore

particles in CZ change with shrinkage ratio or temperature. Finally, the solid conductivity and gas-solid heat transfer coefficient in CZ are specified according to the different heat and mass transfer mechanisms in each of the states. Figure 17 shows that the process model with different CZ treatments predicts different CZ shape and position, and the anisotropic non-layered CZ leads to a higher pressure than those from other treatments. Modeling layered CZ in a BF process models probably becomes common.^[48,50,154]

During BF operation, instabilities may arise from inadequate control of 3D distributions of flow and thermochemical behaviors inside the furnace. Therefore, another important aspect for modeling BF process is to describe 3D characteristics of in-furnace states. Some early 3D BF process models, based on in-house codes, have been reported by de Castro et al.^[150] and Takatani et al.^[153] Recently, de Castro et al.^[51] extended their 3D model to consider six phases (gas, lump solids, hot metal, molten slag, PC, pulverized charcoal), rather than the four phases (gas, solids, liquid, and PC) considered previously.^[69,150] On the other hand, Shen et al.^[52] developed a 3D process model based on ANSYS CFX and linked this model to their raceway model.^[39] With this model, they demonstrated the complicated 3D behaviors of gas and liquid around the raceway (see, for example, Figure 18). These studies represent the encouraging progress in more realistically modeling a BF process. However, in most of the current 3D models, a few important aspects were missing, for example, layered CZ and discrete nature of liquid were not considered fully.

On the other hand, the developed models have been used to investigate different BF operations. For example, Nogami et al.^[155] numerically studied the BF operation with intensive hydrogen injection and found that the coke rate remarkably decreases with the injection, while the converted reducing agent rate shows small change. Kuang et al.^[47] modified the model of Dong et al.^[46] to consider the stockline variation which is inevitable in practice, and then by use of this modified model, assessed hot burden charge operation under different conditions. Li et al.^[156] studied the interactions of BF inner profile with operational condition and material properties, and obtained different trends for the effect of the throat-to-belly diameter ratio on BF performance for different productivities. Zhang et al.^[157–159] examined the flow and thermochemical behaviors in an oxygen BF and found that the magnetite reserve zone wherein the composition of iron ore remains steady is significantly reduced by the strongly reducing atmosphere compared to the conventional BF. Chu and his colleagues^[160–164] analyzed the usage of different technologies such as top gas recycling, hot burden charging, injection of coke oven gas and natural gas, and their different combinations, which provides detailed evidence for the implementation of these technologies in aspects of the in-furnace state and global performance.

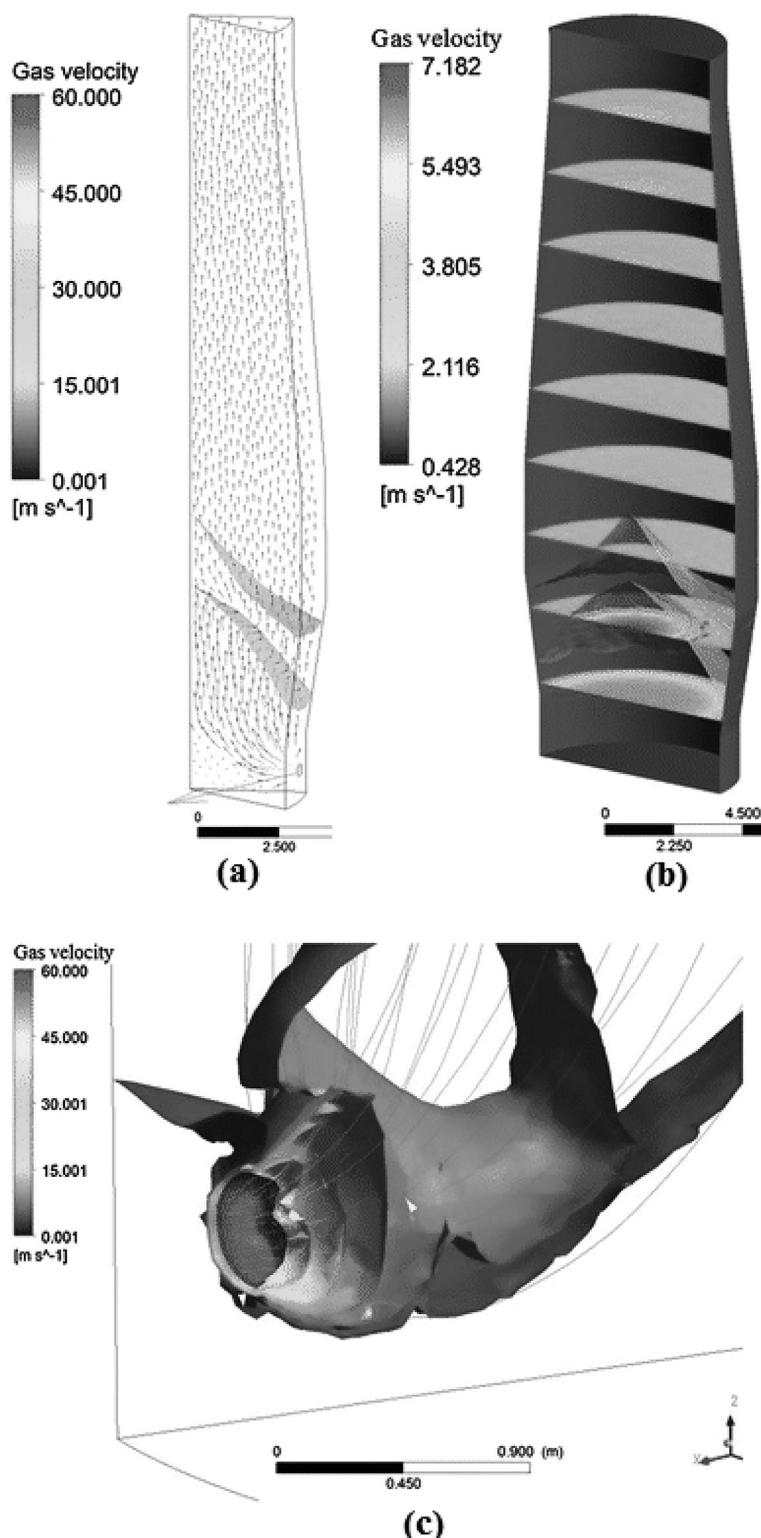


Figure 18. Flow pattern of gas velocity: a), along the central vertical plane; b), contour on horizontal slices at different heights; and c), over the localized iso-surfaces of gas velocity.^[52]

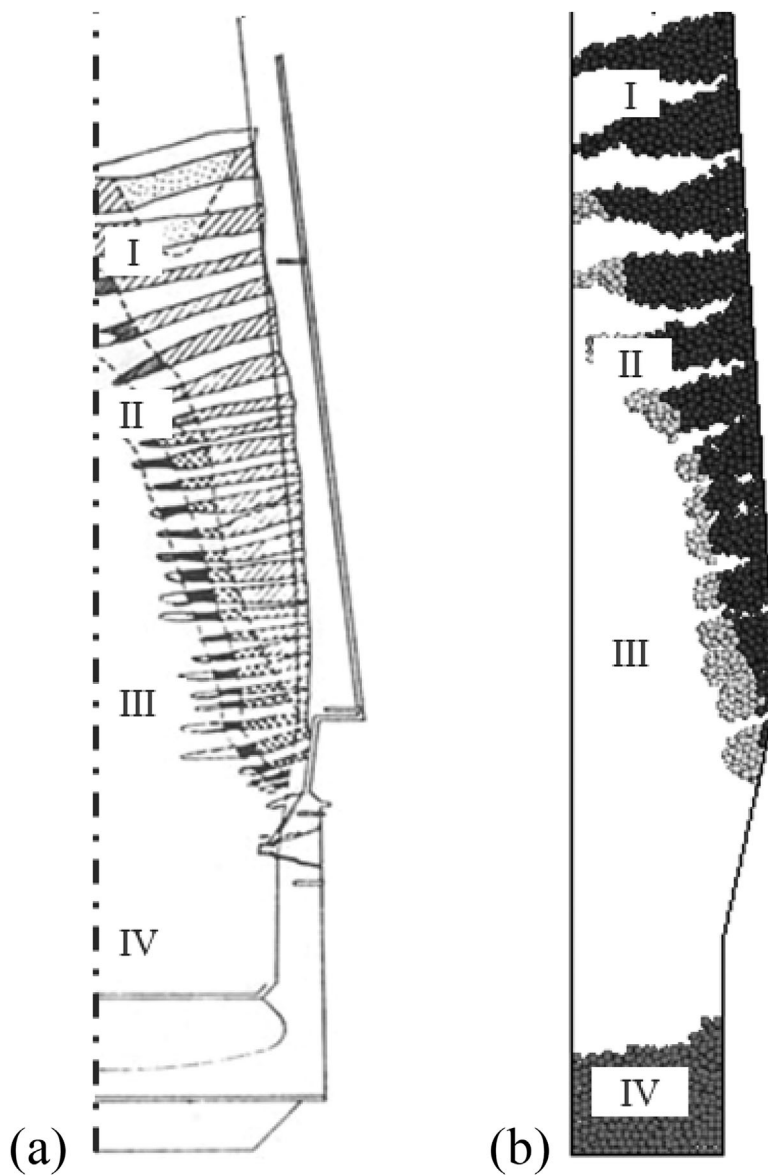


Figure 19. In-furnace state of different zones: a) from a dissection study (I: layered structure; II: CZ including fused layers; III: coke zone and the deadman; IV: hearth)^[167] and b) from the present particle scale simulation (Coke particles above the hearth are not shown).^[62]

3.4.3.2. Discrete Modeling: At present, the process models to describe the coupled flow, heat and mass transfer inside BFIs by discrete approaches are still under development and only few studies have been reported. Yang et al.^[54] proposed a new approach to describe the behaviors of wax beads corresponding to ore in a CZ. In their model, the porosity of particles varies with Yong's Modulus, which is expressed as a function of temperature. This new approach, although being, thus, far verified at much lower temperatures than those within a real BF, can in principle be applied to ore particles with the support of physical experiments, which eliminates the arbitrary treatment of ore

softening and melting behaviors in the DEM modeling of BFIs. Natsui et al.^[165] modeled the flow, heat and mass transfer in a simplified cylindrical reactor by a 3D CFD-DEM model and considered the iron ore reduction by CO. Later, this model was extended to include the reduction by H₂.^[59] Peters and Hoffmann^[61] developed a 1D CFD-DEM model to investigate iron ore reduction against the measurement. Recently, based on the comprehensive heat transfer model of Zhou et al.,^[166] Hou et al.^[62] developed a 2D CFD-DEM model to simulate the multiphase flow and thermochemical behaviors and performance of the LKAB experimental BF. This model can satisfactorily predict gas and solid

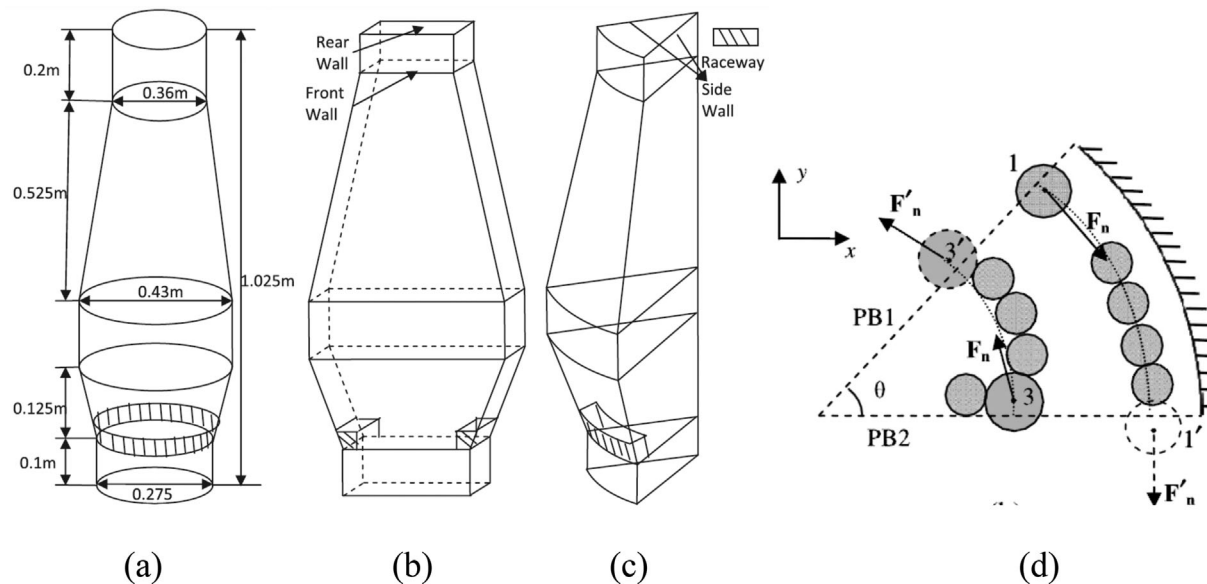


Figure 20. Simulated blast furnace geometries of a) full 3D model, b) slot model, and c) sector model, together with d) circumferential periodic boundary conditions (PBC) for particles.^[63]

temperature against the measurements. Furthermore, it can reproduce different flow zones in the BF, including the shape and position of CZ, as shown in Figure 19. This development, although promising, does not explicitly model the liquid flow and raceway combustion. Also, it introduces an initial CZ position to avoid considering the

entire processing time in one cycle, which is about 4 h for one cycle in practice. Thus, the transient behaviors of individual particles from the onset of reduction reactions to their melting into liquid cannot be considered. To overcome these problems, more research efforts are apparently needed.

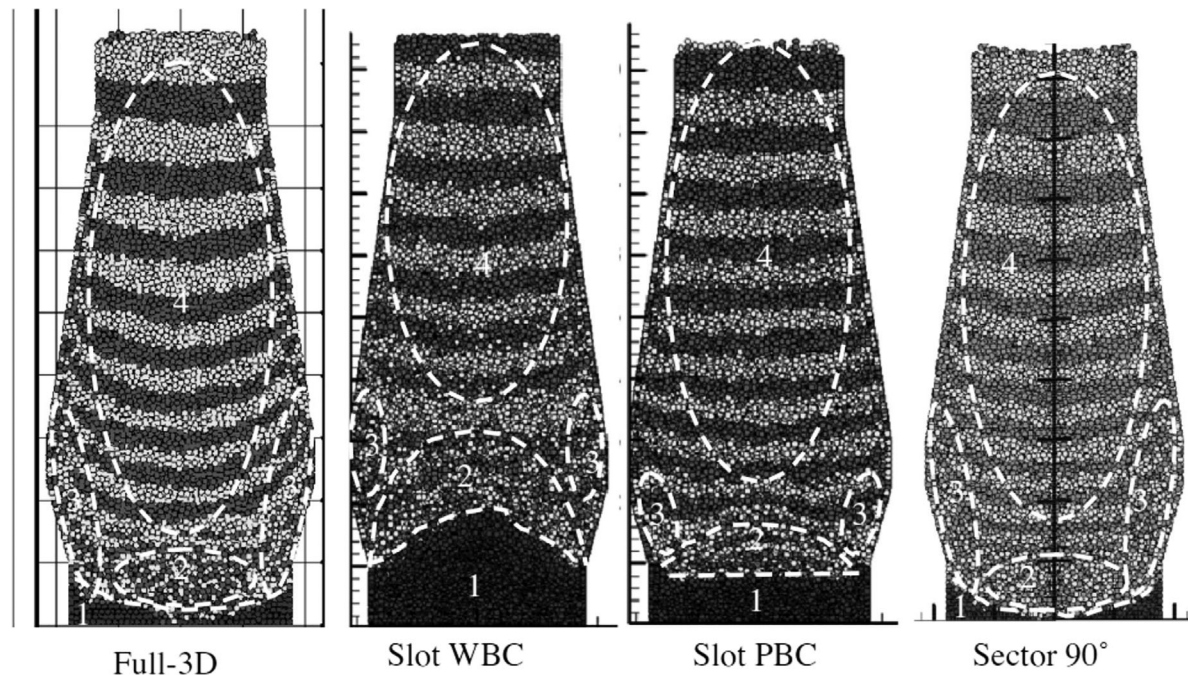


Figure 21. Steady solid flow pattern in the 2D and 3D models: 1—stagnant zone, 2—quasi-stagnant zone, 3—funnel flow, and 4—plug flow.^[63]

4. Large-Scale Simulation

Practical BFs can have an inner volume of up to 6000 m³, involving in billions of particles. Simulation of such a large-scale problem by DEM/CFD-DEM approach is extremely time demanding. To overcome this problem, a few developments in aspects of modeling technique and computer technology have been recently made.

4.1. Modeling Techniques

To date, the majority of discrete BF models are based on 2D slot model to reduce the computational demand. However, it may experience significant deviation from the reality.^[63] Under a normal operation, the flows along the circumference can largely be regarded symmetrical and thus only a part of the furnace along this direction needs to be simulated. In this respect, a comprehensive CFD-DEM sector model, facilitated with circumferential periodic boundary conditions (see Figure 20), has been recently developed to describe the gas-solid flow in the BF.^[63] As shown in Figure 21, this sector model can produce the solid flow patterns close to those given by a full 3D model, which cannot be achieved by the 2D slot models. This has also been confirmed, when different pre-set cohesive zones are considered.^[63]

Another potential method to reduce the computation loading of discrete model is to use a “scaled” method in simulations. In the past, many discrete simulations of particulate systems including BF simply scale up particle size and/or scale down the computational domain without any theoretical base. Also, the so called coarse-grain models have been introduced for DEM-based simulations, where a particle assembly is represented by a number of original particles and a scaling law is derived according to the force balance between a coarse-grain or parcel particle and corresponding original particles.^[168,169] However, this treatment needs to estimate the physical properties of a coarse-grain particle and there is no theoretical base to do so. As such, significant efforts are needed to develop various scale-up and scale-down theories to speed up the simulations of practical BFs.

4.2. GPU Computing Technology

With the rapid improvement of computer hardware performance, GPU (Graphic Process Unit) has emerged to not only render 3D scene, but also support more and more complicated computations. In the discrete simulation of granular flow, the overall speed-up ratio of GPU parallel codes to its serial CPU counterparts is reported to be from several times to tens of times. More importantly, by use of multiple GPUs, simulating systems with millions of particles is becoming realistic for engineering applications.^[64,170] This has been recently demonstrated by Gan et al.^[64] who simulated the bell-less top

charging process with rotating chute for a practical BF by their generalized-purpose GPU-based DEM model and reduced the simulation time from one month (for CPU-based simulation) to only one day by a single GPU. Therefore, GPU technology can drastically speed up the discrete and continuum simulations of BF processes. It should be pointed out that the use of GPU for a simulation does not change the equations of the mathematical model involved. The resulting high computational performance is achieved through the special hardware architectures and control processes.^[171] Such control generally becomes more challenging for the complicated systems like BF, where many phases co-exist and experience intensive interactions with each other in terms of flow and heat and mass transfer. These interactions cause significant communications between phases during a simulation. They, if being improperly treated, may massively decrease the extent of GPU acceleration. To date, GPU-based simulations have mainly focused the flows within relatively simple systems involving one or two phases. Its application to BF simulation is very few and should be explored further in the future.

5. Conclusion Remarks

Multi-scale phenomena associated with ironmaking BF raise the needs for modeling this reactor at different time and length scales. In this direction, both continuum and discrete models, and their combinations as well, have been extensively developed to study the transport phenomena within a BF from the top charging system to the hearth. From the review of these studies, especially those conducted recently, the following conclusions can be drawn.

1. Continuum approach plays a dominating role in the mathematical modeling of BF processes, which may continue in the foreseen future. Various continuum models have been developed to predict important local phenomena, such as raceway formation and combustion, drainage of liquid slag and iron, hearth lining erosion, CZ formation, burden descent, and powder accumulation, respectively. Also, multi-fluid continuum process models, which predict the flow and thermochemical behaviors inside the main body and the global performance of a BF, have been developed. The usefulness of these models has been demonstrated through various studies of conventional and new BF operations. Recent efforts have been focused on the description of the local and global phenomena under more realistic conditions, such as layered burden structure, 3D in-furnace states, interactions between different phenomena.
2. The continuum-based models introduce more or less global assumptions and arbitrary treatments due to the lack of reliable constitutive correlations, especially for the solid phase. To overcome this difficulty, there is a need to do more research about granular materials,

- as recognized in the community.^[172] Interestingly, the expected constitutive correlations can in principle be developed using proper averaging theory from the microscopic information generated by discrete simulations. How to generalize this approach represents a challenge in the future studies. More importantly, in the framework of continuum modeling of a BF process, the top charging system and raceway can be simplified as inlet boundary conditions and hearth as outlet boundary conditions, so that they can be modeled separately. This has been the case and proven to be effective in the past. However, the integrated combination of the process model with the burden charging, hearth and raceway sub-models is necessary in order to better solve practical problems. Such research would represent an important need in developing comprehensive continuum-based models.
3. Discrete approach is very attractive for BF research because of its inherent nature for reliably describing the particles behaviors that play a dominating role inside a BF. In recent years, it has been widely used to study the solid flow patterns and related gas behaviors, especially the formation of stagnant zone and its state relative to liquid drainage, raceway formation, effects of CZ shape and position, and abnormal phenomena resulting from wall scaffold and tuyere closure. More recently, discrete-based models have also been developed to predict the liquid trickling flow, as well as the coupled multiphase flow, heat and mass flow behaviors in a BF.
 4. There are, however, various challenges in developing comprehensive and useful discrete-based BF process models, for example, in effectively describing the softening and melting behaviors of iron ore, the flow and thermochemical behavior of discrete droplets/rivulets, and the coke and coal combustion in tuyeres/raceways. Also, discrete simulations are computationally very demanding, which necessitates not only the use of advanced GPU computing technology, but also the development of general scale theories to reduce the computational effort. All these represent an important research area in the future.

Acknowledgments

The authors are grateful to the Australian Research Council (ARC) (IH140100035) and the Natural Science Foundation of China (NSFC) (91534206 and U1560205) for the financial support of the work.

Received: February 26, 2017; Revised: June 6, 2017;
Published online: July 7, 2017

Keywords: blast furnace; heat and mass transfer; mathematical modeling; multiphase flow; numerical simulation

References

- [1] A. Orth, N. Anastasijevic, H. Eichberger, *Miner. Eng.* **2007**, *20*, 854.
- [2] C. B. Xu, D. Q. Cang, *J. Iron Steel Res. Int.* **2010**, *17*, 1.
- [3] A. Babich, H. W. Gudenhau, K. Mavrommatis, C. Froehling, A. Formoso, A. Cores, L. Garcia, *Rev. Metal. Madrid* **2002**, *38*, 288.
- [4] A. K. Biswas, *Principles of Blast Furnace Ironmaking: Theory and Practice*, Cootha Publishing House, Brisbane, Australia **1981**.
- [5] Y. Omori, *Blast Furnace Phenomena and Modelling*, Elsevier Applied Science, New York, USA **1987**.
- [6] Y. Tsuji, *Chem. Eng. Sci.* **2007**, *62*, 3410.
- [7] H. P. Zhu, Z. Y. Zhou, R. Y. Yang, A. B. Yu, *Chem. Eng. Sci.* **2007**, *62*, 3378.
- [8] H. P. Zhu, Z. Y. Zhou, R. Y. Yang, A. B. Yu, *Chem. Eng. Sci.* **2008**, *63*, 5728.
- [9] Z. Y. Zhou, S. B. Kuang, K. W. Chu, A. B. Yu, *J. Fluid Mech.* **2010**, *661*, 482.
- [10] J. Yagi, *ISIJ Int.* **1993**, *33*, 619.
- [11] X. F. Dong, A. B. Yu, J. Yagi, P. Zulli, *ISIJ Int.* **2007**, *47*, 1553.
- [12] S. Ueda, S. Natsui, H. Nogami, J. Yagi, T. Ariyama, *ISIJ Int.* **2010**, *50*, 914.
- [13] T. Ariyama, S. Natsui, T. Kon, S. Ueda, S. Kikuchi, H. Nogami, *ISIJ Int.* **2014**, *54*, 1457.
- [14] K. Takatani, T. Inada, K. Takata, *ISIJ Int.* **2001**, *41*, 1139.
- [15] K. Nishioka, T. Maeda, M. Shimizu, *ISIJ Int.* **2005**, *45*, 669.
- [16] T. Nouchi, M. Sato, K. Takeda, T. Ariyama, *ISIJ Int.* **2005**, *45*, 1515.
- [17] Y. Zhang, R. Deshpande, D. Huang, P. Chaubal, C. Q. Zhou, *Int. J. Heat Mass Transfer* **2008**, *51*, 186.
- [18] J. Brännbacka, H. Saxén, *Ind. Eng. Chem. Res.* **2008**, *47*, 7793.
- [19] B. Y. Guo, D. Maldonado, P. Zulli, A. B. Yu, *ISIJ Int.* **2008**, *48*, 1676.
- [20] M. Iida, K. Ogura, T. Hakone, *ISIJ Int.* **2009**, *49*, 1123.
- [21] C. Q. Zhou, D. Huang, Y. F. Zhao, P. Chaubal, *J. Therm. Sci. Eng. Appl.* **2010**, *2*, 011006.
- [22] B. Y. Guo, P. Zulli, D. Maldonado, A. B. Yu, *Metall. Mater. Trans. B* **2010**, *41*, 876.
- [23] B. Y. Guo, A. B. Yu, P. Zulli, D. Maldonado, *Steel Res. Int.* **2011**, *82*, 579.
- [24] L. Shao, H. Saxén, *Steel Res. Int.* **2012**, *83*, 878.
- [25] L. Shao, H. Saxén, *Ind. Eng. Chem. Res.* **2013**, *52*, 5479.
- [26] W. T. Cheng, E. N. Huang, S. W. Du, *Int. Commun. Heat Mass* **2014**, *57*, 13.
- [27] K. M. Komiyama, B. Y. Guo, H. Zughbi, P. Zulli, A. B. Yu, *Metall. Mater. Trans. B* **2014**, *45*, 1895.
- [28] K. M. Komiyama, B. Y. Guo, H. Zughbi, P. Zulli, A. B. Yu, *Steel Res. Int.* **2015**, *86*, 592.
- [29] H. Saxén, *Metall. Mater. Trans. B* **2015**, *46*, 421.

- [30] B. Y. Guo, P. Zulli, H. Rogers, J. G. Mathieson, A. B. Yu, *ISIJ Int.* **2005**, *45*, 1272.
- [31] S. S. Mondal, S. K. Som, S. K. Dash, *J. Phys. D: Appl. Phys.* **2005**, *38*, 1301.
- [32] C. W. Chen, *Appl. Math. Model.* **2005**, *29*, 871.
- [33] S. Sarkar, G. S. Gupta, S. Y. Kitamura, *ISIJ Int.* **2007**, *47*, 1738.
- [34] T. Umekage, M. Kadokawa, S. Yuu, *ISIJ Int.* **2007**, *47*, 659.
- [35] Y. S. Shen, B. Y. Guo, A. B. Yu, D. Maldonado, P. Austin, P. Zulli, *ISIJ Int.* **2008**, *48*, 777.
- [36] Y. S. Shen, B. Y. Guo, A. B. Yu, P. Zulli, *Fuel* **2009**, *88*, 255.
- [37] Y. S. Shen, D. Maldonado, B. Y. Guo, A. B. Yu, P. Austin, P. Zulli, *Ind. Eng. Chem. Res.* **2009**, *48*, 10314.
- [38] M. Y. Gu, G. Chen, M. C. Zhang, D. Huang, P. Chaubal, C. Q. Zhou, *Appl. Math. Model.* **2010**, *34*, 3536.
- [39] Y. S. Shen, B. Y. Guo, A. B. Yu, P. R. Austin, P. Zulli, *Fuel* **2011**, *90*, 728.
- [40] D. Fu, D. Z. Zheng, C. Q. Zhou, J. D'Alessio, K. J. Ferron, Y. F. Zhao, Parametric studies on PCI performances, Proceedings of the ASME/JSME 2011: 8th Thermal Engineering Joint Conference, Honolulu, Hawaii, United States, March 13-17, 2011.
- [41] A. T. Wijayanta, M. S. Alam, K. Nakaso, J. Fukai, K. Kunitomo, M. Shimizu, *ISIJ Int.* **2014**, *54*, 1521.
- [42] D. Rangarajan, T. Shiozawa, Y. S. Shen, J. S. Curtis, A. B. Yu, *Ind. Eng. Chem. Res.* **2014**, *53*, 4983.
- [43] Y. S. Shen, A. B. Yu, *Steel Res. Int.* **2015**, *86*, 604.
- [44] T. Okosun, S. J. Street, J. Zhao, B. Wu, C. Q. Zhou, *Ironmaking Steelmaking* **2016**, <https://doi.org/10.1080/03019233.2016.1217116>
- [45] Z. Miao, Z. Y. Zhou, A. B. Yu, Y. S. Shen, *Powder Technol.* **2017**, *314*, 542.
- [46] X. F. Dong, A. B. Yu, S. J. Chew, P. Zulli, *Metall. Mater. Trans. B* **2010**, *41*, 330.
- [47] S. B. Kuang, Z. Y. Li, D. L. Yan, Y. H. Qi, A. B. Yu, *Miner. Eng.* **2014**, *63*, 45.
- [48] D. Fu, Y. Chen, Y. F. Zhao, J. D'Alessio, K. J. Ferron, C. Q. Zhou, *Appl. Therm. Eng.* **2014**, *66*, 298.
- [49] D. Fu, Y. Chen, C. Q. Zhou, *Appl. Math. Model.* **2015**, *39*, 7554.
- [50] P. Zhou, H. L. Li, P. Y. Shi, C. Q. Zhou, *Appl. Therm. Eng.* **2016**, *95*, 296.
- [51] J. A. de Castro, A. J. da Silva, Y. Sasaki, J. Yagi, *ISIJ Int.* **2011**, *51*, 748.
- [52] Y. S. Shen, B. Y. Guo, S. J. Chew, P. Austin, A. B. Yu, *Metall. Mater. Trans. B* **2015**, *46*, 432.
- [53] L. Kempton, D. Pinson, S. J. Chew, P. Zulli, A. B. Yu, *Powder Technol.* **2012**, *223*, 19.
- [54] W. J. Yang, Z. Y. Zhou, D. Pinson, A. B. Yu, *Metall. Mater. Trans. B* **2015**, *46*, 977.
- [55] S. Ueda, T. Kon, H. Kurosawa, S. Natsui, T. Ariyama, H. Nogami, *ISIJ Int.* **2015**, *55*, 1232.
- [56] S. Natsui, T. Kikuchi, R. O. Suzuki, T. Kon, S. Ueda, H. Nogami, *ISIJ Int.* **2015**, *55*, 1259.
- [57] T. Kon, S. Natsui, S. Ueda, H. Nogami, *ISIJ Int.* **2015**, *55*, 1284.
- [58] S. Natsui, R. Nashimoto, T. Kikuchi, R. O. Suzuki, H. Takai, K. I. Ohno, S. Sukenaga, *AIChE J.* **2017**, *63*, 2257.
- [59] S. Natsui, T. Kikuchi, R. O. Suzuki, *Metall. Mater. Trans. B* **2014**, *45*, 2395.
- [60] S. Natsui, H. Takai, R. Nashimoto, T. Kikuchi, R. O. Suzuki, *Int. J. Heat Mass Transfer* **2015**, *91*, 1176.
- [61] B. Peters, F. Hoffmann, *Chem. Eng. J.* **2016**, *304*, 692.
- [62] Q. F. Hou, E. Dianyu, S. B. Kuang, Z. Y. Li, A. B. Yu, *Powder Technol.* **2017**, *314*, 557.
- [63] W. J. Yang, Z. Y. Zhou, A. B. Yu, *Chem. Eng. J.* **2015**, *278*, 339.
- [64] J. Q. Gan, Z. Y. Zhou, A. B. Yu, *Powder Technol.* **2016**, *301*, 1172.
- [65] S. A. Zaïmi, T. Akiyama, J. B. Guillot, J. Yagi, *ISIJ Int.* **2000**, *40*, 322.
- [66] H. P. Zhu, Z. Y. Zhou, A. B. Yu, P. Zulli, *Granul. Matter* **2009**, *11*, 269.
- [67] Z. Y. Zhou, H. P. Zhu, B. Wright, A. B. Yu, P. Zulli, *Powder Technol.* **2011**, *208*, 72.
- [68] J. Chen, T. Akiyama, H. Nogami, J. Yagi, H. Takahashi, *ISIJ Int.* **1993**, *33*, 664.
- [69] P. R. Austin, H. Nogami, J. Yagi, *ISIJ Int.* **1997**, *37*, 458.
- [70] H. Jin, S. Choi, J. Yagi, J. Chung, *ISIJ Int.* **2010**, *50*, 1023.
- [71] S. Ergun, A. A. Orning, *Ind. Eng. Chem.* **1949**, *41*, 1179.
- [72] Q. H. Zeng, A. B. Yu, G. Q. Lu, *Ind. Eng. Chem. Res.* **2010**, *49*, 12793.
- [73] Q. J. Zheng, Z. Y. Zhou, A. B. Yu, *Powder Technol.* **2013**, *248*, 25.
- [74] L. W. Rong, K. J. Dong, A. B. Yu, *Chem. Eng. Sci.* **2014**, *116*, 508.
- [75] B. H. Xu, A. B. Yu, S. J. Chew, P. Zulli, *Powder Technol.* **2000**, *109*, 13.
- [76] Z. Y. Zhou, H. P. Zhu, A. B. Yu, B. Wright, D. Pinson, P. Zulli, *ISIJ Int.* **2005**, *45*, 1828.
- [77] Z. Y. Zhou, H. P. Zhu, A. B. Yu, B. Wright, P. Zulli, *Comput. Chem. Eng.* **2008**, *32*, 1760.
- [78] Z. Zhou, H. Zhu, A. Yu, P. Zulli, *ISIJ Int.* **2010**, *50*, 515.
- [79] H. Mio, M. Kadokawa, S. Matsuzaki, K. Kunitomo, *Miner. Eng.* **2012**, *33*, 27.
- [80] S. Kikuchi, T. Kon, S. Ueda, S. Natsui, R. Inoue, T. Ariyama, *ISIJ Int.* **2015**, *55*, 1313.
- [81] S. J. Zhang, A. B. Yu, P. Zulli, B. Wright, U. Tuzun, *ISIJ Int.* **1998**, *38*, 1311.
- [82] H. P. Zhu, A. B. Yu, *Phys. Rev. E* **2002**, *66*, 021302.
- [83] K. Shibata, Y. Kimura, M. Shimizu, S. Inaba, *ISIJ Int.* **1990**, *30*, 208.

- [84] A. K. Vats, S. K. Dash, *Ironmaking Steelmaking* **2000**, 27, 123.
- [85] V. Panjkovic, J. S. Truelove, P. Zulli, *Ironmaking Steelmaking* **2002**, 29, 390.
- [86] W. T. Cheng, C. N. Huang, S. W. Du, *Chem. Eng. Sci.* **2005**, 60, 4485.
- [87] B. Desai, R. V. Ramna, S. K. Dash, *ISIJ Int.* **2006**, 46, 1396.
- [88] C. E. Huang, S. W. Du, W. T. Cheng, *ISIJ Int.* **2008**, 48, 1182.
- [89] C. M. Chang, W. T. Cheng, C. E. Huang, S. W. Du, *Int. Commun. Heat Mass* **2009**, 36, 480.
- [90] M. Swartling, B. Sundelin, A. Tilliander, P. Jönsson, *Steel Res. Int.* **2010**, 81, 724.
- [91] S. Kumar, *ISIJ Int.* **2005**, 45, 1122.
- [92] M. Swartling, B. Sundelin, A. Tilliander, P. G. Jönsson, *Steel Res. Int.* **2010**, 81, 186.
- [93] T. Nouchi, A. B. Yu, K. Takeda, *Powder Technol.* **2003**, 134, 98.
- [94] T. Nouchi, K. Takeda, A. B. Yu, *ISIJ Int.* **2003**, 43, 187.
- [95] T. Nouchi, T. Sato, M. Sato, K. Takeda, T. Ariyama, *ISIJ Int.* **2005**, 45, 1426.
- [96] K. Nishoka, T. Maeda, M. Shimizu, *ISIJ Int.* **2005**, 45, 1496.
- [97] K. Nishioka, T. Maeda, M. Shimizu, *ISIJ Int.* **2005**, 45, 1506.
- [98] L. Shao, H. Saxén, *ISIJ Int.* **2013**, 53, 988.
- [99] L. Shao, H. Saxén, *ISIJ Int.* **2011**, 51, 228.
- [100] L. Shao, H. Saxén, *Steel Res. Int.* **2012**, 83, 197.
- [101] L. Shao, H. Saxén, *ISIJ Int.* **2013**, 53, 1756.
- [102] J. Brännbacka, J. Torrkulla, H. Saxén, *Ironmaking Steelmaking* **2005**, 32, 479.
- [103] S. K. Dash, D. N. Jha, S. K. Ajmani, A. Upadhyaya, *Ironmaking Steelmaking* **2004**, 31, 207.
- [104] Y. L. Li, S. S. Cheng, P. Zhang, S. H. Zhou, *ISIJ Int.* **2015**, 55, 2332.
- [105] M. Zagaria, V. Dimastromatteo, V. Colla, *Ironmaking Steelmaking* **2010**, 37, 229.
- [106] M. X. Feng, R. Chen, Q. Li, *Mater. Res. Innov.* **2015**, 19, 448.
- [107] Y. F. Zhao, D. Fu, L. W. Lherbier, Y. Chen, C. Q. Zhou, J. G. Grindley, *Steel Res. Int.* **2014**, 85, 891.
- [108] Y. Q. Feng, D. Pinson, A. B. Yu, S. J. Chew, P. Zulli, *Steel Res. Int.* **2003**, 74, 523.
- [109] H. Nogami, H. Yamaoka, K. Takatani, *ISIJ Int.* **2004**, 44, 2150.
- [110] S. Yuu, T. Umekage, T. Miyahara, *ISIJ Int.* **2005**, 45, 1406.
- [111] T. Umekage, S. Yuu, M. Kadokawa, *ISIJ Int.* **2005**, 45, 1416.
- [112] J. E. Hilton, P. W. Cleary, *Chem. Eng. Sci.* **2012**, 80, 306.
- [113] Q. F. Hou, E. Dianyu, A. B. Yu, *AIChE J.* **2016**, 62, 4240.
- [114] R. Murai, M. Sato, T. Ariyama, *ISIJ Int.* **2004**, 44, 2168.
- [115] S. W. Du, W. H. Chen, *Int. Commun. Heat Mass* **2006**, 33, 327.
- [116] A. T. Wijayanta, M. S. Alam, K. Nakaso, J. Fukai, K. Kunitomo, M. Shimizu, *Fuel Process. Technol.* **2014**, 117, 53.
- [117] Y. S. Shen, A. B. Yu, *Miner. Eng.* **2016**, 90, 89.
- [118] Y. S. Shen, B. Y. Guo, A. B. Yu, P. Zulli, *ISIJ Int.* **2009**, 49, 819.
- [119] Y. S. Shen, A. B. Yu, P. R. Austin, P. Zulli, *Powder Technol.* **2012**, 223, 27.
- [120] J. H. Liao, A. B. Yu, Y. S. Shen, *Powder Technol.* **2017**, 314, 550.
- [121] V. R. Radhakrishnan, K. Maruthy Ram, *J. Process Control* **2001**, 11, 565.
- [122] S. Nag, S. Basu, A. B. Yu, *Ironmaking Steelmaking* **2009**, 36, 509.
- [123] Z. J. Teng, S. S. Cheng, P. Y. Du, X. B. Guo, *Int. J. Miner. Met. Mater.* **2013**, 20, 620.
- [124] T. Mitra, H. Saxén, *ISIJ Int.* **2016**, 56, 1570.
- [125] S. D. Liu, Z. Y. Zhou, K. J. Dong, A. B. Yu, D. Pinson, J. Tsalapatis, *Steel Res. Int.* **2015**, 86, 651.
- [126] C. K. Ho, S. M. Wu, H. P. Zhu, A. B. Yu, S. T. Tsai, *Miner. Eng.* **2009**, 22, 986.
- [127] H. Mio, S. Komatsuki, M. Akashi, A. Shimosaka, Y. Shirakawa, J. Hidaka, M. Kadokawa, H. Yokoyama, S. Matsuzaki, K. Kunitomo, *ISIJ Int.* **2010**, 50, 1000.
- [128] Y. W. Yu, A. Westerlund, T. Paananen, H. Saxén, *ISIJ Int.* **2011**, 51, 1050.
- [129] Y. W. Yu, H. Saxén, *Ind. Eng. Chem. Res.* **2012**, 51, 7383.
- [130] Y. W. Yu, H. Saxén, *Steel Res. Int.* **2013**, 84, 1018.
- [131] J. L. Zhang, J. Y. Qiu, H. W. Guo, S. Ren, H. Sun, G. W. Wang, Z. K. Gao, *Particuology* **2014**, 16, 167.
- [132] Y. W. Yu, H. Saxén, *Powder Technol.* **2014**, 262, 233.
- [133] S. A. Załmi, T. Akiyama, J. B. Guillot, J. Yagi, *ISIJ Int.* **2000**, 40, 332.
- [134] H. Nogami, J. Yagi, *ISIJ Int.* **2004**, 44, 1826.
- [135] S. J. Zhang, A. B. Yu, P. Zulli, B. Wright, P. Austin, *Appl. Math. Model.* **2002**, 26, 141.
- [136] Z. Y. Zhou, A. B. Yu, P. Zulli, *Prog. Comput. Fluid Dyn.* **2004**, 4, 39.
- [137] R. S. Nick, A. Tilliander, T. L. I. Jonsson, P. G. Jönsson, *ISIJ Int.* **2013**, 53, 979.
- [138] G. X. Wang, A. B. Yu, P. Zulli, *ISIJ Int.* **1997**, 37, 441.
- [139] G. X. Wang, S. J. Chew, A. B. Yu, P. Zulli, *ISIJ Int.* **1997**, 37, 573.
- [140] G. X. Wang, D. Y. Liu, J. D. Litster, A. B. Yu, S. J. Chew, P. Zulli, *Chem. Eng. Sci.* **1997**, 52, 4013.
- [141] G. X. Wang, S. J. Chew, A. B. Yu, P. Zulli, *Metall. Mater. Trans. B* **1997**, 28, 333.
- [142] G. X. Wang, J. D. Litster, A. B. Yu, *ISIJ Int.* **2000**, 40, 627.
- [143] S. J. Chew, P. Zulli, A. B. Yu, *ISIJ Int.* **2001**, 41, 1112.
- [144] S. J. Chew, P. Zulli, A. B. Yu, *ISIJ Int.* **2001**, 41, 1122.
- [145] S. J. Chew, P. Zulli, D. Maldonado, A. B. Yu, *ISIJ Int.* **2003**, 43, 304.

- [146] X. F. Dong, A. B. Yu, J. M. Burgess, D. Pinson, S. J. Chew, P. Zulli, *Ind. Eng. Chem. Res.* **2009**, *48*, 214.
- [147] S. Koshizuka, Y. Oka, *Nucl. Sci. Eng.* **1996**, *123*, 421.
- [148] K. Nishioka, K. Ohno, T. Maeda, M. Shimizu, *Recent Progress on Mathematical Modeling in Ironmaking 2008*, ISIJ, Tokyo **2008**.
- [149] T. Kon, S. Natsui, S. Ueda, R. Inoue, T. Ariyama, *ISIJ Int.* **2012**, *52*, 1565.
- [150] J. A. de Castro, H. Nogami, J. Yagi, *ISIJ Int.* **2002**, *42*, 44.
- [151] H. Nogami, M. S. Chu, J. Yagi, *Comput. Chem. Eng.* **2005**, *29*, 2438.
- [152] P. R. Austin, H. Nogami, J. Yagi, *ISIJ Int.* **1997**, *37*, 748.
- [153] K. Takatani, T. Inada, Y. Ujisawa, *ISIJ Int.* **1999**, *39*, 15.
- [154] K. Yang, S. Choi, J. Chung, J. Yagi, *ISIJ Int.* **2010**, *50*, 972.
- [155] H. Nogami, Y. Kashiwaya, D. Yamada, *ISIJ Int.* **2012**, *52*, 1523.
- [156] Z. Y. Li, S. B. Kuang, D. L. Yan, Y. H. Qi, A. B. Yu, *Metall. Mater. Trans. B* **2017**, *48*, 602.
- [157] Z. L. Zhang, J. L. Meng, L. Guo, Z. C. Guo, *JOM* **2015**, *67*, 1945.
- [158] Z. L. Zhang, J. L. Meng, L. Guo, Z. C. Guo, *JOM* **2015**, *67*, 1936.
- [159] Z. L. Zhang, J. L. Meng, L. Guo, Z. C. Guo, *Metall. Mater. Trans. B* **2016**, *47*, 467.
- [160] M. S. Chu, J. Yagi, *Steel Res. Int.* **2010**, *81*, 1043.
- [161] T. L. Guo, M. S. Chu, Z. G. Liu, J. Tang, J. Yagi, *Steel Res. Int.* **2013**, *84*, 333.
- [162] T. L. Guo, M. S. Chu, Z. G. Liu, H. T. Wang, *J. Iron Steel Res. Int.* **2014**, *21*, 729.
- [163] Z. Liu, M. Chu, T. Guo, H. Wang, X. Fu, *Ironmaking Steelmaking* **2016**, *43*, 64.
- [164] H. T. Wang, M. S. Chu, T. L. Guo, W. Zhao, C. Feng, Z. G. Liu, J. Tang, *Steel Res. Int.* **2016**, *87*, 539.
- [165] S. Natsui, R. Shibasaki, T. Kon, S. Ueda, R. Inoue, T. Ariyama, *ISIJ Int.* **2013**, *53*, 1770.
- [166] Z. Y. Zhou, A. B. Yu, P. Zulli, *AIChE J.* **2009**, *55*, 868.
- [167] S. Watakabe, K. Miyagawa, S. Matsuzaki, T. Inada, Y. Tomita, K. Saito, M. Osame, P. Sikstrom, L. S. Okvist, J. O. Wikstrom, *ISIJ Int.* **2013**, *53*, 2065.
- [168] M. Sakai, S. Koshizuka, *Chem. Eng. Sci.* **2009**, *64*, 533.
- [169] K. W. Chu, J. Chen, A. B. Yu, *Miner. Eng.* **2016**, *90*, 43.
- [170] J. Xu, H. B. Qi, X. J. Fang, L. Q. Lu, W. Ge, X. W. Wang, M. Xu, F. G. Chen, X. F. He, J. H. Li, *Particuology* **2011**, *9*, 446.
- [171] D. B. Kirk, W.-M. W. Hwu, *Programming Massively Parallel Processors: A Hands-on Approach*, Elsevier Science & Technology, San Francisco, USA **2012**.
- [172] H. M. Jaeger, S. R. Nagel, *Science* **1992**, *255*, 1523.